

1 Biogeophysical feedbacks enhance the Arctic terrestrial 2 carbon sink in regional Earth system dynamics

3

4 **Wenxin Zhang¹, Christer Jansson², Paul A Miller¹, Benjamin Smith¹, Patrick
5 Samuelsson²**

6 [1]{Department of Physical Geography and Ecosystem Science, Lund University, SE-223 62
7 Lund, Sweden}

8 [2]{Rossby Centre, Swedish Meteorological and Hydrological Institute, SE-601 76,
9 Norrköping, Sweden}

10 Correspondence to: W. Zhang (zhang_wenxin2005@hotmail.com)

11 **Abstract**

12 Continued warming of the Arctic will likely accelerate terrestrial carbon (C) cycling by
13 increasing both uptake and release of C. Yet, there are still large uncertainties in modelling
14 Arctic terrestrial ecosystems as a source or sink of C. Most modelling studies assessing or
15 projecting the future fate of C exchange with the atmosphere are based on either stand-alone
16 process-based models or coupled climate-C cycle general circulation models, and often
17 disregard biogeophysical feedbacks of land surface changes to the atmosphere. To understand
18 how biogeophysical feedbacks might impact on both climate and the C budget in Arctic
19 terrestrial ecosystems, we apply the regional Earth system model RCA-GUESS over the
20 CORDEX-Arctic domain. The model is forced with lateral boundary conditions from an EC-
21 Earth CMIP5 climate projection under the RCP 8.5 scenario. We perform two simulations,
22 with or without interactive vegetation dynamics respectively, to assess the impacts of
23 biogeophysical feedbacks. Both simulations indicate that Arctic terrestrial ecosystems will
24 continue to sequester C with an increased uptake rate until the 2060-70s, after which the C
25 budget will return to a weak C sink as increased soil respiration and biomass burning outpaces
26 increased net primary productivity. The additional C sinks arising from biogeophysical
27 feedbacks are approximately 8.5 Gt C, accounting for 22% of the total C sinks, of which
28 83.5% are located in areas of extant Arctic tundra. Two opposing feedback mechanisms,
29 mediated by albedo and evapotranspiration changes respectively, contribute to this response.
30 The albedo feedback dominates in the winter and spring seasons, amplifying the near-surface

31 warming by up to 1.35 °C in spring, while the evapotranspiration feedback dominates in the
32 summer months, and leads to a cooling of up to 0.81 °C. Such feedbacks stimulate vegetation
33 growth due to an earlier onset of the growing-season, leading to compositional changes in
34 woody plants and vegetation redistribution.

35 **1 Introduction**

36 Satellite-derived indices, plot-scale surveys and modelling experiments suggest that Arctic
37 terrestrial ecosystems have undergone structural and compositional changes in response to
38 widespread environmental changes in recent decades (Beck and Goetz, 2011; Elmendorf et
39 al., 2012; Miller and Smith, 2012). Vegetation change in turn feeds back to climate via
40 alterations in biogeochemical forcing (e.g. changes in carbon (C) or nutrient cycling that
41 affect greenhouse gases (GHG) emissions) or biogeophysical properties of the land surface
42 such as albedo, roughness length, and partitioning of return energy fluxes from the surface
43 into latent and sensible heat components (Cox et al., 2000; Brovkin et al., 2006).
44 Biogeophysical feedbacks are particularly important for the northern high latitudes (NHLs).
45 Positive albedo feedbacks arising from an expansion and densification of shrublands and
46 forests or from snow-masking by protruding branches and leaves have a large potential to
47 amplify regional climate warming (Chapin et al., 2005; Bonfils et al., 2012). Moreover,
48 biogeophysical feedbacks associated with coupled climate-vegetation dynamics will be linked
49 to biogeochemical feedbacks to the atmosphere through their influence on the terrestrial C
50 and water cycles (Bonan, 2008). Most modelling studies assessing or projecting the state of
51 the C budget for Arctic tundra or the NHLs are based on either stand-alone process-based
52 models or coupled climate-carbon cycle general circulation models (GCMs), also known as
53 Earth system models (ESMs) (Sitch, 2008; Qian et al., 2010; McGuire et al., 2012). In
54 general, these studies disregard biogeophysical feedbacks likely to modify initial climate
55 forcing substantially at the local or regional scale under high GHG emission scenarios and
56 consequently affect biogeochemical cycling. In this regard, it is critical to understand the role
57 of biogeophysical feedbacks for both Arctic climate change and terrestrial ecosystems' C
58 balance, especially if their impact on near-surface temperatures is, as some estimates indicate,
59 of a similar order of magnitude as biogeochemical mechanisms (Betts, 2000; Bathiany et al.,
60 2010).

61

62 **1.1 Filling gaps in biogeophysical feedback loops by employing a regional** 63 **Earth system model**

64 Traditionally, C stores and fluxes simulated by dynamic vegetation models (DVMs) reflect
65 passive responses of terrestrial ecosystems to spatial and temporal variations in climate, since
66 such climate is generated by climate models which often represent vegetation as either a static
67 or an asynchronous dynamic component in the climate system (Quillet et al., 2010). To fill
68 gaps in the biogeophysical feedback loops relies on climate models being tightly coupled with
69 DVMs, which can often trigger cascading impacts to amplify or dampen climate change
70 (Fig.1). When it comes to Arctic tundra or the NHLs, enhanced solar radiation absorption and
71 near-surface warming are expected to directly stimulate plants' photosynthesis, leading to
72 increased leaf area index (LAI) in the growing season (Piao et al., 2006), and eventually to
73 change vegetation composition and distribution, such as occurs, for example, with a
74 northward invasion of trees and tall shrubs into extant tundra areas (Tape et al., 2006; Miller
75 & Smith, 2012). Ecosystems comprised of taller plants with bigger leaves have higher
76 vegetation roughness, and can accentuate vertical mixing of eddy fluxes, resulting in more
77 efficient transport of momentum, heat and moisture from the canopy to the atmosphere.
78 Accordingly, a negative feedback loop is signified by increased latent heat fluxes, cooling the
79 surface by reducing sensible heating or by weakening atmospheric heating due to a greater
80 abundance of low clouds. On the other hand, invading vegetation or increased LAI may
81 darken the surface, particularly through shading of snow in late winter and spring, and reduce
82 surface albedo, leading to a positive feedback to near-surface temperature. Previous studies of
83 vegetation feedbacks to precipitation have been inconclusive, with indications of positive,
84 negative and minimal feedbacks (Seneviratne et al., 2010; Keuper et al., 2012), but they are
85 likely associated with factors such as wetness of ecosystems, enhanced evapotranspiration and
86 soil moisture, convective characteristics of climate and land surface heterogeneities.

87 Recently, ESMs have started to include interactive vegetation dynamics in their land surface
88 components in order to fully address the effects of both biogeochemical and biogeophysical
89 feedbacks arising from land cover change and land management practices (e.g. Bathiany et
90 al., 2010; Falloon et al., 2012). However, some processes that occur on a wide range of spatial
91 scales might not be well represented due to their rather coarse resolution. For example,
92 Lorant et al. (2013) pointed out that consistent declines in albedo with increasing tree cover,
93 occurring south of latitudinal tree-line, are poorly represented by ESMs, partly because of

94 their relatively coarse resolution. Regional climate models (RCMs) are complementary tools
95 to GCMs, providing high-resolution simulations of the climate over a limited domain forced
96 by GCM-derived fields on the lateral domain boundaries. By accounting for physiographic
97 features such as mountain chains, lakes and coastlines in a more detailed way, they tend to
98 provide more reliable local or regional details of climate information to end-users and policy-
99 making communities (Rummukainen, 2010). Kueppers et al. (2005) showed that a RCM-
100 based climate projection is more suitable for predictions of potential shifts in species' ranges
101 than GCM-based climate projections in California, since land surface properties, topography,
102 climatologically distinct ecoregions, and local climate variations with distance from the coast
103 are better resolved in the RCM outputs. To better capture biogeophysical feedbacks to climate
104 resulting from vegetation structural changes, Smith et al. (2011) first coupled the individual-
105 based DVM LPJ-GUESS to a RCM. In a case study over Europe, Wramneby et al. (2010)
106 demonstrated both albedo- and evapotranspiration-mediated feedbacks, and found that
107 biogeophysical feedbacks to future warming were relatively modest compared to the radiative
108 forcing of increased global CO₂ concentrations.

109 **1.2 Present studies of terrestrial C balance for Arctic tundra and the NHLs**

110 Arctic tundra and boreal forests have sequestered a considerable amount of C during historic
111 and recent geological times (Oechel et al., 1993; Ruckstuhl et al., 2008). However, the
112 current, recent and future C balance of Arctic terrestrial ecosystems is still under debate due
113 to the large uncertainties associated with the various methodologies used to estimate regional
114 C fluxes or due to the large sensitivities associated with various controlling mechanisms (e.g.
115 gradients of climatic and hydrological variability, disturbances, permafrost vulnerability and
116 nutrient constraints) (Hayes et al., 2012). CO₂ flux measurements indicate that warm winters
117 tend to switch old boreal stands from a sink to a source of C by increasing annual respiration
118 (Valentini et al., 2000; Monson et al., 2006). Similarly, studies using remote sensing
119 approaches have identified a trend of decreasing boreal forest productivity in parts of the
120 Arctic in recent years (Beck and Goetz, 2011). By contrast, results of GCM simulations from
121 the Coupled Carbon Cycle Climate Model Intercomparison Project (C4MIP) indicate that the
122 NHLs will be a C sink of 0.3 ± 0.3 Pg C yr⁻¹ by 2100 (Qian et al., 2010). Forest inventory data
123 and long-term ecosystem C studies estimate that boreal forests were a sink for atmospheric
124 CO₂ on the order of 0.5 ± 0.08 Pg C yr⁻¹ in both the 1990s and 2000s (Pan et al., 2011). Most
125 of this C was stored as increases in dead wood, litter, and soil C pools in Russia. More

126 recently, a compilation of flux observations and inversion model estimates for Arctic tundra
127 indicate that large uncertainties in the annual exchange of CO₂ between Arctic tundra and the
128 atmosphere cannot distinguish the Arctic terrestrial C budget from neutral balance (McGuire
129 et al., 2012).

130 Biogeophysical feedbacks involving plant-mediated changes in albedo, evapotranspiration,
131 surface roughness and energy flux partitioning affect the efficiency of the terrestrial biosphere
132 as a sink for CO₂ from the atmosphere. The ESMs studies generally agree that biogeophysical
133 feedbacks to climate warming are positive for the NHL and are likely give rise to an amplified
134 warming in the future (Falloon et al., 2012). However, the amplified warming is also likely to
135 have positive and counteracting effects on both vegetation net primary productivity (NPP) and
136 soil heterotrophic respiration (HR). These responses increase uncertainties in determining
137 whether Arctic terrestrial ecosystems will be a sink or source of C under future climate
138 change.

139 In this study, we highlight the importance of including interactive vegetation dynamics in
140 simulations of the future Arctic climate. To this end, we employ a regional ESM (RCA-
141 GUESS) that couples a regional climate model (RCA4) with an individual-based dynamic
142 vegetation-ecosystem model (LPJ-GUESS) to study the coupled evolution of climate,
143 vegetation and ecosystem C balance across the pan-Arctic. By comparing simulations with
144 and without interactive vegetation dynamics forced by lateral boundary conditions from a
145 GCM under a strong future warming scenario (RCP8.5), we analyse how biogeophysical
146 feedbacks arising from distributional and structural change in arctic tundra and boreal forest
147 may impact the Arctic climate and terrestrial C balance. Specifically, we investigate the
148 following questions:

- 149 1. How well does RCA-GUESS simulate Arctic climate, vegetation and C fluxes in the recent
150 period?
- 151 2. How do biogeophysical feedbacks affect Arctic climate and terrestrial C balance in a
152 warmer, high-CO₂ future climate?
- 153 3. What aspects of vegetation change are particularly associated with changes in terrestrial C
154 balance?

155 **2 Methods**

156 **2.1 RCA-GUESS, a regional Earth system model**

157 RCA-GUESS (Smith et al. 2011) is a regional ESM, in which the Land Surface Scheme
158 (LSS) of the regional climate model RCA4 is coupled with dynamic vegetation and
159 ecosystem biogeochemistry simulated by the individual-based vegetation-ecosystem model
160 LPJ-GUESS.

161 RCA refers to the Rossby Centre Atmosphere regional climate model that has been modified
162 and updated mostly with respect to the parameterization of physical land-surface processes
163 dealing with physiography and cold climate conditions in mid- and high-latitudes
164 (Samuelsson et al., 2011). The LSS in RCA uses separate tiles for forest and open land. The
165 forest tile is further subdivided into fractions for canopy and forest floor and the proportion of
166 broad-leaved versus needle-leaved (coniferous) forest. The open land tile has separate
167 fractions for vegetation and bare soil. When snow is present, both tiles have a fraction of
168 snow covering the ground. All fractions have their own surface energy balance which are
169 weighted together to provide grid-averaged radiative and turbulent fluxes as surface boundary
170 conditions required by the atmospheric numerical model (Samuelsson et al., 2006).

171 The Lund-Potsdam-Jena General Ecosystem Simulator (LPJ-GUESS) is an individual-based
172 vegetation-ecosystem model optimized to resolve heterogeneities of vegetation structures and
173 functions at the regional and continental scale (Smith et al., 2001). It shares mechanistic
174 formulations for canopy biophysics, phenology, plant physiology and ecosystem C cycling
175 with the global vegetation model LPJ-DGVM (Sitch et al., 2003) and incorporates improved
176 formulations of ecosystem hydrology (Gerten et al., 2004). However, it differs from the
177 generalized large-area parameterization of vegetation structure and population dynamics used
178 in LPJ-DGVM, adopting instead gap model formalisms based on explicit representations of
179 growth and competition among cohort-averaged woody plant individuals and a herbaceous
180 understory co-occurring within patches differing in age-since-last-disturbance. Woody plants
181 and herbaceous vegetation are parameterized by Plant Functional Types (PFTs), which are
182 parameter sets governing plant traits with regard to morphology, phenology, shade and
183 drought tolerance, fire resistance and bioclimatic limits. LPJ-GUESS has been successfully
184 applied to model dynamic changes of potential natural vegetation (PNV) across biomes of the
185 world, including Europe (e.g. Hickler et al., 2012), and Arctic and Subarctic regions (e.g.

186 Zhang et al., 2013a). The performance and behaviour of the model in simulating ecosystem
187 carbon cycle variations and responses to drivers has been highlighted, for example, by
188 Ahlström et al. (2012a, b), Piao et al. (2013) and Smith et al. (2014).

189 In RCA-GUESS, the vegetation dynamics affects the LSS of RCA by dynamically adjusting
190 the LAI and the relative cover of needle-leaved and broad-leaved forests in the forest tile and
191 herbaceous vegetation in the open land tile. In this study, the 6 global PFTs used in LPJ-
192 GUESS consist of boreal needle-leaved evergreen trees (e.g. *Picea obovata*, *Picea abies*),
193 boreal shade-intolerant needle-leaved evergreen trees (e.g. *Pinus sylvestris*), boreal needle-
194 leaved deciduous trees (e.g. *Larix sibirica*), temperate broad-leaved deciduous trees (e.g. *Tilia*
195 *cordata*), boreal shade-intolerant broad-leaved deciduous trees (e.g. *Betula pubescens*) and C3
196 grass (e.g. *Gramineae*). The parameter sets for characteristic traits of PFTs are given in Table
197 S1 in the Supplement. The simulated daily LAI and phenology state of the needle-leaved and
198 broad-leaved PFTs in LPJ-GUESS are aggregated to the corresponding forest types in the
199 forest tile of RCA (Eq. 1.1 in Table S2 in the Supplement). The relative cover fractions of
200 forests and herbaceous vegetation within the forest and open land tile are estimated as the
201 foliar projective cover computed from the simulated LAI using Lambert Beer's law (Eq. 1.2-
202 1.4 in Table S2 in the Supplement). The returned LAI alters the surface and aerodynamic
203 resistances which are further used by RCA for the calculation of the sensible and latent heat
204 fluxes (Eq. 1.5-1.9 in Table S2 in the Supplement). The fractional size of the forest tile is
205 allowed to vary only if the simulated maximum growing-season LAI summed across forest
206 PFTs is lower than 1, signifying marginal or stunted woody plant growth. The relative covers
207 for forests and open land affect the weighted averaged albedo for each grid cell (Eq. 2.0 in
208 Table S2). The configuration and behaviour of RCA-GUESS is described in detail by Smith
209 et al. (2011).

210 **2.2 Model domain, driving data and simulation protocols**

211 The simulations were applied across the Arctic domain of the Coordinated Regional Climate
212 Downscaling Experiment (CORDEX-Arctic). The domain encompasses 150×156 grid points
213 with a uniform resolution of $0.44 \times 0.44^\circ$ (approximately 50 km) by rotating the pole system
214 over an equatorial domain. The boundary conditions were taken from the CMIP5 (Coupled
215 Model Intercomparison Project phase 5) simulations of the EC-Earth GCM (Hazelegger et al.,
216 2010, 2011) for the RCP8.5 scenario (Moss et al., 2010).

217 RCA-GUESS was initialized by a spin-up phase to achieve an equilibrium state for vegetation
218 structure and composition, C pool and climate conditions appropriate to the period 1961-
219 1990. Compared to the relatively short spin-up necessary for RCA (only a few months), LPJ-
220 GUESS requires a much longer spin-up composed of two stages. In the first stage, LPJ-
221 GUESS is run in an un-coupled mode, forced by climate variables (precipitation, sunshine,
222 temperature) from the CRU TS3.0 (1991-2006) (Climate Research Unit Time Series)
223 observation-based climate dataset (Mitchell and Jones, 2005). The first-stage spin-up
224 encompasses 360 years, repeatedly cycling detrended CRU climate from the period 1901-
225 1930 and the 1901 atmospheric CO₂ concentration of 296 ppm until 1900, and thereafter
226 observed climate and CO₂ until 1960. After 1960, the simulation continues for a further 30
227 years but in a coupled mode, with RCA-generated climate fields forcing LPJ-GUESS, while
228 LPJ-GUESS returns vegetation properties to RCA. In the second-stage spin-up, a new 360
229 year spin-up is performed, using a detrended version of the climate forcing generated by RCA
230 for the period 1961-1990 in the first stage. This two-stage procedure to spin up the vegetation
231 model aims to produce a smooth transition of the climate forcing from the uncoupled spin-up
232 to the coupled (RCA-forced) phase of the final simulation, avoiding a step change in the
233 forcing that may initiate drift in the soil and vegetation carbon pool sizes, disrupting the
234 baseline for the subsequent coupled phase of the simulation. After the spin-up phase, RCA-
235 GUESS was run in the coupled mode for the period 1961-1990. Two simulations were then
236 performed for the period 1991-2100 in coupled and un-coupled modes respectively (hereafter
237 referred to as the feedback run and the non-feedback run). In the non-feedback run, RCA was
238 forced by daily mean vegetation properties averaged from the LPJ-GUESS outputs for the
239 period 1961-1990.

240 **2.3 Evaluation of the climate, vegetation and Arctic tundra C balance** 241 **simulated for the recent period**

242 Outputs from RCA-GUESS for the period 1961-1990 were compared with available
243 observational datasets, omitting the relaxation zone around the domain boundary. Seasonal
244 mean 2m temperature and total precipitation (the sum of convective and large-scale
245 precipitation) were obtained from two datasets: the CRU TS3.0 and WILLMOTT 3.02
246 (Willmott and Matsuura, 1995). To evaluate the simulated vegetation distribution, we
247 compared the model-derived dominant PNV map to the map composed using the International
248 Satellite Land Surface Climatology Project (ISLSCP) II PNV Cover dataset and the Kaplan

249 PNV dataset (Kaplan et al., 2003) based on the same aggregated vegetation classes (see Table
250 S3 in the Supplement). The Kaplan PNV dataset supplements the ISLSCP II PNVC dataset
251 with additional details of low and tall shrubs across Arctic tundra. The dominant PNV in the
252 model was derived from the PFT with the largest LAI in each grid cell. The latitudinal
253 percentage difference for each aggregated vegetation type between the composed map and the
254 simulated map is quantified by the number of grid cells in which the simulation over- or
255 underestimates each vegetation type divided by the total number of grid cells in each latitude
256 band. The simulated NPP flux was evaluated using data from both Arctic tundra and boreal
257 forest datasets: the Ecosystem Model-Data Intercomparison (EMDI) (Olson et al., 2013a), the
258 Biological Productivity of Ecosystems of Northern Eurasia (BAZ) (Denissenko et al., 2013),
259 the Global Primary Production Data Initiative Product, R2 (GPPDI_1) (Olson et al., 2013b),
260 the Global Primary Production Data Initiative Product, R3 (GPPDI_2) (Zheng et al., 2013)
261 and the NPP Boreal Forest (BOREAL) (Gower et al., 2012). To evaluate net ecosystem
262 exchange (NEE), the residual difference among the fluxes of NPP, HR and fire disturbance,
263 we compared inter-annual variability of NEE anomalies and mean C budget for an Arctic
264 tundra domain (McGuire et al., 2012; Fig. S1 in the Supplement) to the estimates of process-
265 based models (LPJ GUESS WHyMe (Wania et al., 2009a, b, 2010; Zhang et al., 2013a).
266 Terrestrial Carbon Flux (TCF) model (Kimball et al. 2009), ORCHIDEE (Koven et al. 2009,
267 2011), Terrestrial Ecosystem Model (TEM; version 6.03) (McGuire et al., 2010; Hayes et al.,
268 2011) and inversion models (Peylin et al., 2013) for the period 1990-2006 (for details also see
269 the Appendix in McGuire et al., (2012)).

270 **2.4 Analysis of impacts of biogeophysical feedbacks to climate, the terrestrial** 271 **C budget and vegetation change**

272 The impacts of biogeophysical land-atmosphere feedbacks on Arctic climate were quantified
273 as mean seasonal and monthly anomalies of 2m temperature and total precipitation averaged
274 over the period 2071-2100 in the feedback run relative to the non-feedback run. Anomalies of
275 surface albedo and latent heat flux were calculated to discriminate albedo- from
276 evapotranspiration-mediated feedbacks in their effects on temperature and precipitation.

277 For the future Arctic terrestrial C budget, we calculated mean C stores and fluxes for Arctic
278 tundra and the CORDEX-Arctic domain respectively, and examined the relative contribution
279 of C sinks from Arctic tundra. We also explored how biogeophysical feedbacks affect C

280 exchange by evaluating the magnitude and year of the peak C uptake rate for both Arctic
281 tundra and boreal forests.

282 Climate-induced vegetation shifts were analysed using the anomalies of a normalized
283 phenology index and a normalized physiognomy index (Wramneby et al. 2010; see Eq. 2.1-
284 2.2 in Table S2 in the supplement) based on LAI changes of the simulated PFTs averaged
285 over the period 2071-2100 relative to 1961-1990. Biogeophysical feedback-induced
286 vegetation shifts were characterized as the anomalies of the aforementioned indices for the
287 period 2071-2100 based on the feedback-run relative to the non-feedback run.

288

289 **3 Results**

290 **3.1 The recent Arctic climate, vegetation and C flux**

291 The simulated mean seasonal climate for 1961-1990 shows a cold bias on the order of 2 °C
292 compared to observations in both spring and summer across the entire domain except northern
293 Canada (Fig. 2b, c, f and g). A warm bias on the order of 2 °C occurs over winter in
294 Scandinavia, in autumn in eastern Siberia and for all seasons in northern Canada (Fig. 2a, d, e
295 and h). The most pronounced bias in seasonal temperature is found in eastern Siberia.
296 Greenland is an exception because both the CRU and WILLMOTT datasets are expected to
297 have a significant bias due to poor coverage of measurement sites. The simulated total
298 seasonal precipitation is 5-20 mm higher compared to the validation datasets, with a relatively
299 larger overestimation across the entire domain in spring and autumn (Fig. 3).

300 The vegetation simulated by RCA-GUESS agrees reasonably well with the validation map in
301 terms of spatial distribution and the latitudinal percent difference of grid cells that each
302 aggregated vegetation class occupies. The belt pattern of herbaceous vegetation across
303 mountain ranges in Scandinavia and eastern Siberia is well displayed in both the model-
304 derived map and the validation map (Fig. 4a and b). The latitudinal percent difference by
305 vegetation class is generally lower than 20% (Fig. 4c). The overestimation of deciduous or
306 evergreen forest fractions is offset by the underestimation of the mixed forests fraction. This
307 inconsistency is partly attributed to different definitions of mixed forests in the model and
308 validation map. In the model output, mixed forests is specified in grid cells with herbaceous
309 fraction <50%, and where neither evergreen nor deciduous trees cover fraction is dominant
310 (<33.3%). However, the validated map mixed forests are classed as lands dominated by trees

311 with a percent canopy cover >60% and height exceeding 2 meters, consisting of tree
312 communities with interspersed mixtures or mosaics of deciduous and evergreen types, but
313 none of which exceeds 60% of the landscape (Loveland et al., 2000). Deciduous forests are
314 overestimated for the herbaceous lands at the latitudes 69-73 °N, as a result of a simulated
315 tree-line situated further north in northern Canada and eastern Siberia.

316 The simulated mean annual NPP for 1961-1990 across Arctic tundra areas (Far East Siberia,
317 Alaska, northern Canada, eastern Siberia) is comparable to the validation datasets, and seldom
318 exceeds 200 g C m⁻² yr⁻¹ (Fig. 5a). Averaged over Arctic tundra, the simulated NPP for 1990-
319 2006 is 266 or 268 g C m⁻² yr⁻¹ (Table 1), which is broadly in line with previous estimates
320 (243-252 g C m⁻² yr⁻¹ for 1960s) by the LPJ-DGVM model reported by Sitch et al. (2007). For
321 European forest, simulated NPP exceeds observations by some 200-300 g C m⁻² yr⁻¹ (Fig. S2).
322 This deviation indicates that nitrogen limitation and land use change are also important for
323 predicting European forest NPP, although they were not included in this study. Similar
324 European forest NPP estimations of approximately 500-600 g C m⁻² yr⁻¹ are seen in
325 simulation results with neither nitrogen limitation nor land use change from both coupled
326 RCA-GUESS runs driven by lateral forcing fields from the reanalysis dataset ERA-40 (Smith
327 et al., 2011), and from LPJ-GUESS stand-alone simulations driven with CRU climate (Wolf
328 et al., 2008). The simulated inter-annual variation of NEE anomalies for 1990-2006 from both
329 RCA-GUESS runs fall within the uncertainty ranges of both process-based models and
330 inversion models for Arctic tundra (Fig. 5b). The RCA-GUESS feedback run shows a
331 downward trend similar to the estimates of process-based models (LPJ-GUESS WHyMe,
332 ORCHIDEE, TCF), indicating a slight trend towards increased carbon uptake (Table 1; Fig.
333 S3). In the non-feedback run, the trend is positive, similar to results from TEM and the
334 ensemble mean of inversions estimates. Overall, the mean annual NPP flux exceeds the sum
335 of respiration and wildfire C emissions, resulting in a net sink of C (negative NEE) into the
336 biosphere. Biogeophysical feedbacks have a marginal impact on this net sink, reducing it by
337 some 5% (Table 1).

338 **3.2 Impacts of biogeophysical feedbacks on Arctic climate**

339 The influence of biogeophysical feedbacks on the simulated mean climate for 2071-2100
340 varies seasonally (Fig. 6a-d). The albedo feedback dominates and causes an enhanced
341 warming in winter and spring, with the greatest additional warming of 1.35 °C occurring in
342 spring (Fig. 7a). The evapotranspiration feedback starts to offset the albedo feedback in

343 spring, and reduces the warming by 0.81 °C in summer over the Arctic as a whole, but with
344 only a moderate influence in autumn (Fig. 6a-d and Fig. 7a). The most pronounced
345 amplification of warming (~3 °C) occurs in spring across tundra areas of Siberia and northern
346 Canada. In Fennoscandia, only the Scandes Mountain range is influenced, with some
347 additional warming in winter and cooling in summer, which is in accordance with results
348 reported by Wramneby et al. (2010). The impacts of biogeophysical feedbacks on
349 precipitation are not as noticeable as for temperature. The greatest change in precipitation
350 occurs in summer with an increase of 3.57 mm over land areas (Fig. 6e-h and Fig. 7b). In
351 contrast to the slight albedo decline of around 0.05 in summer, albedo in autumn, winter and
352 spring is reduced significantly across the whole tundra area with the greatest reduction of
353 around 0.2 occurring in spring (Fig. 6i-l). Sporadic increases of albedo are found in the larch
354 forest belt of central Siberia from autumn to spring. An increase in latent heat flux is seen in
355 spring and summer for most land areas except for northern Canada and eastern Siberia, where
356 there is a reduction in magnitude (Fig. 6m-p). The largest latent heat flux increase, 9-15 W m⁻²,
357 is seen mostly in spring, with smaller increases, 1-9 W m⁻², in the summer months.

358 **3.3 Impacts of biogeophysical feedbacks on future Arctic vegetation patterns** 359 **and C budget**

360 The phenological response to the simulated climate change effects on vegetation composition
361 is not consistent across the entire CORDEX-Arctic domain. The Scandes Mountain range,
362 north-western Siberia, eastern Siberia coast and northern Canada show a substantial increase
363 in the relative abundance of evergreen PFTs, but north-eastern Europe, the Taymyr Peninsula,
364 Far East Siberia and the high Canada Arctic show an increased abundance of deciduous PFTs
365 (Fig. 8a). Biogeophysical feedbacks tend to counteract these changes in Far East Siberia, but
366 to reinforce them in the Taymyr Peninsula (Fig. 8b). The poleward transitions from grassy
367 PFTs to woody PFTs indicate that the tree-line boundary moves further north as a result of
368 future climate favourable to the growth of trees (Fig. 8c). Biogeophysical feedbacks further
369 aid the advance of woody plants into Arctic tundra in both Far East Siberia and western
370 Siberia (Fig. 8d). Compared to climate-induced shifts in vegetation abundance, the effects of
371 biogeophysical feedbacks on vegetation distribution are relatively smaller, typically less than
372 30% in terms of changes to the normalized phenology and physiognomy indices (Fig 8b, 8d).

373 The inter-annual variation of the NEE flux for 1991-2100 in the RCA-GUESS non-feedback
374 run indicates that the C uptake rate could start to increase rapidly in the 2020s, reach the

375 largest value in the 2060s, after which the C uptake rate decreases until the 2090s (Fig. 9a).
376 However, in the RCA-GUESS feedback run, the biogeophysical feedbacks further enhance C
377 uptake from the 2020s, and postpone the arrival of the largest C uptake rate for 15 years. To
378 examine where and how many grid cells might exhibit this behaviour, we sorted the grid cells
379 into groups according to the extent of the increase or decrease of the NEE seen in each cell.
380 Most grid cells with the enhanced C uptake are found in Arctic tundra with an increase of
381 NEE around $50\text{-}100\text{ g C m}^{-2}\text{ yr}^{-1}$, while boreal forests show more grid cells with the largest
382 NEE flux decreased by $0\text{-}50\text{ g C m}^{-2}\text{ yr}^{-1}$ (Fig. 9b). Meanwhile, Arctic tundra also includes
383 more grid cells with the largest C uptake rate postponed than boreal forests (Fig. 9c). In total,
384 by the end of 2100, the CORDEX-Arctic domain will gain 38.7 Gt C (Table 2), of which 35.6
385 Gt C is sequestered by Arctic tundra. This estimation is comparable to the estimates of
386 C4MIP simulations of around 38 ± 20 Gt C for the NHLs (Qian et al., 2012). Most of the C
387 gains are allocated to vegetation biomass. Litter and soil C stores are increased by 0.5 and 1.2
388 Gt C respectively for Arctic tundra, but decreased by 1.8 and 6.4 Gt C respectively for the
389 CORDEX-Arctic domain. Biogeophysical feedbacks account for about 22% of the increase in
390 net C uptake, around 8.5 Gt C. The majority (83.5%) of this extra C uptake comes from areas
391 simulated as Arctic tundra in the modern climate.

392 **4 Discussion**

393 **4.1 The robustness of regional climate simulations**

394 The biases within the down-scaled climate in an RCM may be inherited either from the
395 systematic bias of lateral boundary conditions provided by large scale fields of climate
396 forcing or shortcomings in the model's structures, formulations and parameterizations. For
397 example, the warm bias over northern Canada in our simulations year-round during the period
398 1961-1990 is inherited from the GCM-simulated fields on the lateral boundaries of the
399 simulated domain; the EC-Earth output shows a warm bias over this area of 1-4 °C for the
400 1980s, when compared to reanalysis data (Koenigk et al., 2013). For other areas of the
401 Arctic, EC-Earth tends to show a cold bias, attributed to the overestimation of sea ice
402 thickness and extent (Koenigk et al., 2013). This likely explains the cold bias in spring and
403 summer found in our simulations across almost the entire domain. Berg et al. (2013)
404 compared ERA-Interim reanalysis climate data to output from an RCA4 simulation across the
405 Arctic forced by ERA-Interim data on the lateral boundaries, identifying a winter-time warm

406 bias in eastern Siberia and a summer-time cold bias across the entire domain. Our simulations
407 show similar patterns.

408 When similar patterns of bias recur in simulations using different lateral forcings, this may
409 indicate the effects of inaccurate parameterizations in the model. Samuelsson et al., (2011)
410 pointed out that RCA4 generally underestimates snow albedo in cold climate regions,
411 resulting in higher air temperatures and less snow accumulation. This probably explains the
412 most pronounced areas of warm bias which occur in eastern Siberia in our simulations.

413 Whereas the bias pattern for temperature is relatively similar between RCA-GUESS and EC-
414 Earth, precipitation bias indicates more inconsistency. For instance, RCA-GUESS simulates
415 less precipitation in the basins of Barents Sea and Bering Strait compared to EC-Earth. This
416 may reflect the greater topographical variability arising from a finer grid resolution in the
417 regional model; in EC-Earth, smoother topography reduces orographic rainfall, potentially
418 spreading the same total amount of precipitation over a larger area, causing overestimation
419 over rainshadow areas in the lee of the mountain ranges. By contrast, RCA4 is known to
420 overestimate precipitation over mountain tops due to an overestimated cloud fraction
421 (Samuelsson et al., 2011). In general, complex mountainous terrain poses a challenge for
422 accurately simulating vertical velocities in the resolved scale. Overall, in comparison to the
423 EC-Earth outputs and observation-based datasets, RCA-GUESS generally demonstrates good
424 skill in reproducing spatial patterns of the present day climate with respect to temperature and
425 precipitation.

426 To verify that our climate simulation set-up, including boundary conditions from EC-Earth
427 and the dynamic down-scaling by the atmospheric component of RCA-GUESS, was leading
428 to representative behaviour in the biogeochemical part of the model, we compare our
429 simulated results for NEE, averaged across the Arctic, with the estimates from stand-alone
430 simulations of LPJ-GUESS forced by a wide range of GCMs under the same (RCP8.5)
431 radiative forcing scenario. Fig. S4 compares the results from this study with results obtained
432 by Ahlström et al. (2012b) in simulations with LPJ-GUESS forced by 18 GCMs from the
433 CMIP5 initiative. The inter-annual variations of the cumulative NEE flux simulated in both
434 the feedback and non-feedback runs agree well with the ensemble mean of the stand-alone
435 simulations from 1990 to 2020. From 2020-2100, the C uptake started to increase more
436 rapidly, but remained within the ensemble range (Fig. S4). This suggests that our climate

437 forcing set-up is representative for climate projections from a wide range of GCMs in terms
438 of predicting the NEE flux.

439 **4.2 Vegetation dynamics and ecosystem biogeochemistry in response to** 440 **Arctic climate change**

441 Distinct geographical patterns of vegetation distribution in the Arctic and NHLs are largely
442 shaped by spatial patterns in temperature and precipitation, while other factors like soil
443 properties, topographical barriers, land use change, and permafrost vulnerability are additional
444 determinants (Morales et al, 2005; Koca et al., 2006; Jiang et al., 2012). Zhang et al. (2013a)
445 demonstrated that LPJ-GUESS shows a generally good performance in replicating vegetation
446 patterns across the Arctic, in particular capturing forest–shrub–tundra transitions observed in
447 the Canadian Arctic, northern Alaska, the Taymyr Peninsula, and the Scandes Mountain range
448 under the present-day climate. RCA-GUESS simulates vegetation shifts in broad agreement
449 with previous studies: the combined effects of climatic warming and elevated CO₂ allow the
450 bioclimatic niche for boreal or temperate forests to move towards higher latitudes and
451 elevations (Fig. 8c; Morales et al., 2007; Wolf et al., 2008; Zhang et al., 2013a); the longer
452 and warmer growing-season favours broad-leaved deciduous (e.g. birch) forests in
453 competition with evergreen forests dominated by species of spruce and pine, typical for the
454 boreal zone (Fig. 8a and c; Hickler et al., 2012; Miller and Smith; 2012; Jiang et al., 2012);
455 and warmer winters and altered precipitation patterns result in boreal deciduous (larch) trees
456 in Siberia giving way to boreal evergreen and temperate deciduous trees (Fig. 8a; Kaplan et
457 al., 2003; Shuman et al., 2011; Zhang et al., 2013a).

458 Numerous modelling studies have explored how climate-, CO₂- and land use-driven variations
459 in NPP, HR and disturbance fluxes might influence the future fate of the present-day sink of
460 atmospheric CO₂ within the terrestrial biosphere (e.g. Ahlström et al., 2012b; Brovkin et al.,
461 2006; Poulter et al., 2011;). Our simulated mean NEE flux averaged from 1990-2006 for
462 Arctic tundra in response to recent climate forcing is similar to other process-based models
463 (Table 1 and Fig. 5b), implying that both coupled and un-coupled process-based models agree
464 that NPP is rising faster than soil respiration in response to near-surface warming. The inter-
465 annual variation of NEE anomalies among all the models do not deviate too much from the
466 ensemble mean of inversion model (top-down) estimates, because they are well constrained
467 by the relative strength of compartment fluxes. For instance, ORCHIDEE determines the high
468 end of the uncertainty range of estimated NPP and RH, while RCA-GUESS simulates more

469 fire disturbances resulting in a larger inter-annual variation (Table 1). RCA-GUESS and LPJ-
470 GUESS WHyMe share the same fire process description, in which fires are determined by the
471 amount of above-ground litter and a soil moisture threshold (Sitch et al., 2003). However,
472 LPJ-GUESS WHyMe is forced by the observation-based, CRU climate dataset and uses an
473 extended set of Arctic-specific PFTs, which depicts the simulated tree-line boundary with
474 more accuracy (Zhang et al., 2013a). The rapid increase of C uptake from the 2020s in both
475 RCA-GUESS runs can be attributed to substantial climate-induced vegetation shifts and a
476 prolonged growing-season length. However, C gains eventually decline as the increased HR
477 flux in response to continuous climate warming outpaces the increased NPP flux. Previous
478 studies based on the stand-alone simulations with DVMs show similar effects (e.g. Cao and
479 Woodard 1998; Cramer et al., 2001; Wolfgang et al., 2006; Zhang et al., 2013a).

480 **4.3 Impacts of biogeophysical feedbacks for future Arctic climate and C** 481 **balance**

482 The net impacts of biogeophysical feedbacks to future climate result largely from the
483 opposing effects of albedo- and evapotranspiration-feedback mechanisms. Firstly, the
484 amplified warming occurring in winter and spring is associated with positive feedbacks
485 arising from substantial reductions of albedo (Fig 6a, b, i and j). Winter- and spring-time
486 albedo reductions indicate that the underlying snow is masked and shaded by stems and
487 leaves of woody vegetation, which increases both in areal extent and local density, resulting
488 in an earlier onset of the growing-season and a longer snow-free season in the future. Based
489 on a non-linear relationship between albedo and summer vegetation biomass, Euskirchen et
490 al. (2009) predicted that the increase of regional summer heat absorption due to potential
491 vegetation change under future climate scenarios (A2, B1 and B2) would be $0.34 \pm 0.23 \text{ W m}^{-2}$
492 decade^{-1} , which is relatively small compared to the corresponding change expected due to a
493 shorter snow season ($3.3 \pm 1.24 \text{ W m}^{-2} \text{ decade}^{-1}$). Assuming our summer albedo decline
494 mainly reflects the contribution from vegetation change, our results are a little larger than
495 their estimates. The decline of summer albedo by 0.05 causes $5\text{-}10 \text{ W m}^{-2}$, or $0.45\text{-}0.90 \text{ W m}^{-2}$
496 decade^{-1} , in the summer heat absorption for 2071-2100 relative to 1961-1990 (Fig. S5).
497 However, it should be noted that the estimates of Euskirchen et al. (2009) are based on stand-
498 alone, uncoupled simulations and use a lower CO_2 concentration scenario. After accounting
499 for the effects of climate-vegetation interaction and stronger CO_2 fertilization, their estimates
500 would be expected to increase. Secondly, attenuated warming in summer is associated with

501 negative feedbacks arising from increased evapotranspiration that overtake positive feedbacks
502 arising from a reduction in albedo. The evapotranspiration is enhanced by a higher overall
503 LAI (leaf surface for evaporation) as well as a denser forest cover, which increases surface
504 roughness, promoting a more dynamic exchange of water vapour and energy with the
505 atmosphere. Kasurinen et al. (2014) analysed latent heat measurement data gathered at 65
506 boreal and arctic eddy-covariance sites and found that from tundra to forests, latent heat flux
507 in summer increases from ~ 75 to $\sim 90 \text{ W m}^{-2}$, which is also in line with our estimates (Fig.
508 6o). On an annual basis, the net effect of these feedbacks on temperature averages a modest
509 $0.0069 \text{ }^\circ\text{C yr}^{-1}$ over the period 1991-2100. As for their effects on the seasonal cycle of Arctic
510 vegetation, however, the feedbacks result in an earlier, longer and more uniform vegetation
511 period, in terms of growing-season temperatures (Fig. 7a), promoting a substantial increase in
512 vegetation productivity. Studies with other global ESMs have reported comparable near-
513 surface temperature increases due to vegetation-mediated feedbacks of around $0.0028 \text{ }^\circ\text{C yr}^{-1}$
514 from the 1870s to the 2080s for the NHLs as a whole (Falloon et al., 2012).

515 Using an iterative coupling approach, Matthes et al. (2011) investigated the sensitivity of
516 projected regional climate change to vegetation shifts imposed on the land surface conditions
517 in a regional climate model (HIRHAM) applied across the Arctic. They found that woody
518 vegetation expansion under an SRES A1B emission scenario led to a change in temperature
519 by $3 \text{ }^\circ\text{C}$ in winter and $-1.5 \text{ }^\circ\text{C}$ in summer. These temperature adjustments were larger than
520 effects attributed to freezing/thawing of soil or insulation by top organic soil horizons.

521 Similarly, we also found the largest warming to occur in winter in areas experiencing gradual
522 dynamic shifts from tundra to forest tundra or forest tundra to forest.

523 The sensitivity of vegetation distribution to the effects of biogeophysical feedbacks seems
524 relatively modest (Fig. 8b and d). The additional C sinks arising from biogeophysical
525 feedbacks correspond, at around 8.5 Gt C , to global anthropogenic emissions for about one
526 year under present conditions (Table 2), relatively modest compared to some estimates of the
527 potential losses of C from thawing permafrost across the Arctic (Schuur et al. 2013). A
528 prolonged growing-season, denser forest cover and invasion of trees into tundra result in even
529 greater enhancements to vegetation productivity, which postpones the arrival of the peak C
530 uptake rate for Arctic terrestrial ecosystems. In our study, dramatic changes were found in the
531 transition from herbaceous to woody vegetation occurring in Arctic tundra (Fig. 8c). These

532 changes appear to primarily account for the simulated increased C storage in areas classified
533 as Arctic tundra in the present climate.

534 **4.4 Perspectives to improve regional ESMs**

535 Our results highlight the significance of implementing biogeophysical mechanisms of
536 climate-vegetation interactions in regional Earth system dynamics. Not only do
537 biogeophysical feedbacks result in a more rapid warming on an annual average basis, but they
538 also cause adjustments in the timing and character of the growing-season that affect
539 vegetation productivity and net C balance, with further implications for climate evolution.
540 However, we do make some simplistic assumptions in this first trial of modelling regional
541 Earth system dynamics over the Arctic, and there are some issues that warrant further
542 investigation in order to improve our understanding of impacts of biogeophysical feedbacks
543 on Arctic terrestrial ecosystems and their C balance.

544 Biogeophysical feedback loops should be expanded to involve energy and water flux
545 exchanged over Arctic sea surface. Swann et al. (2010) advanced a hypothesis in which a
546 positive albedo feedback prompts the growth of vegetation, leading to an increased flux of
547 water vapour to the atmosphere, thereby strengthening radiative forcing. After being mixed in
548 the atmosphere, water vapour feeds back on climate not only over land but also over the sea
549 surface, triggering a subsequent positive sea ice feedback, which in turn warms the land
550 surface. They found radiative forcing from water vapour changes to be of a similar magnitude
551 as the direct short-wave forcing from albedo reductions. Therefore, further modelling studies
552 on Arctic regional Earth system dynamics ought to include the ocean component to fully
553 address biogeophysical feedbacks.

554 Permafrost C feedbacks due to future climate change should be considered when terrestrial
555 biogeochemical cycling is coupled with biogeophysical mechanisms. Enormous amounts of
556 organic C stored in the NHL permafrost soils could become vulnerable to decomposition, and
557 act as a positive feedback to accelerate climate warming (Koven et al., 2011; MacDougall et
558 al., 2012). Most terrestrial C cycling models including our model do not have representations
559 of permafrost C dynamics, and thus may neglect the contributions to future climate change
560 from this substantial amount of C. Recent expert assessments estimate permafrost C release
561 for the RCP 8.5 scenario to be 162-288 Pg C by 2100 (Schuur et al., 2013). Environmental
562 change affected by biogeophysical feedbacks could either mitigate or exacerbate permafrost

563 degradation associated with the projected warming. Changes in regional patterns of
564 precipitation and extra warming due to albedo- and evapotranspiration-feedbacks will likely
565 change soil water content and temperatures, affecting the absolute and relative amounts of
566 CO₂ and CH₄ released to the atmosphere. The cooling effects of shading by shrubs in Arctic
567 tundra may reduce summer permafrost thaw, even though continued warming of the Arctic
568 may offset this negative feedback in the long term (Blok et al., 2010). Other factors such as
569 snow redistribution, snow depth changes, and changes to shrub height, cover and expansion
570 are also important in order to quantify the net effects of climate-vegetation interactions on
571 permafrost thermal dynamics (Lawrence and Swenson, 2011). Increased efforts are needed to
572 have an overall understanding of the link between permafrost C and biogeophysical
573 mechanisms.

574 Discrepancies between the simulated and actual vegetation distribution can be overcome by
575 considering factors such as land use change and more detailed vegetation types. Wramneby et
576 al., (2010) found that land use change from croplands to forests and abandoned lands would
577 impact the strength of the albedo- and evapotranspiration-mediated feedbacks over Europe. In
578 mountainous areas, land-use change plays an even more important role in driving tree-line
579 dynamics than climate change (Hickler et al., 2012). For Arctic ecosystem dynamics,
580 terrestrial ecosystem models should be tailored to better capture a variety of Arctic and
581 Subarctic landscapes, and include tall and low shrubs, graminoid forbs, lichen and moss. In
582 this study, using C3 grass and trees instead of forbs and shrubs typical for Arctic tundra, we
583 may underestimate the C uptake strength arising from shrubs' expansion despite our model's
584 ability to capture the grass-wood transition in a manner similar to the forests-shrubs-tundra
585 transition seen in Zhang et al., (2013a). Moreover, it is important to evaluate the algorithm to
586 derive albedo change from simulated changes in vegetation relative cover fractions and LAI.
587 Brovkin et al. (2013) present an approach to evaluate woody vegetation cover and land
588 surface albedo in ESMs that can be applied to regional studies as well.

589 The model version adopted for this study does not include nutrient feedbacks to vegetation
590 growth, although N cycling is included in the current offline version of LPJ-GUESS (Smith et
591 al., 2014). Nitrogen mineralisation rates in the cold soils of boreal and Arctic ecosystems are
592 known to limit the productivity of vegetation in these areas. Simulations with N-enabled
593 global carbon cycle models generally suggest that C sequestration under a future high CO₂
594 climate will be lower globally when N-cycle feedbacks are accounted for (Zaehle and

595 Dalmonech, 2011). However, increasing mineralisation rates in warming soils will reduce N-
596 limitation, allowing substantial productivity increases as growing seasons become longer and
597 warmer. In addition, trees colonising tundra areas rendered accessible by a milder climate
598 constitute a temporary, new sink for carbon until stand carrying capacity is reached and
599 mortality matches biomass growth. As shown for the N-enabled version of LPJ-GUESS by
600 W  rlind et al. (2014), these effects will counteract any tendency for N availability to inhibit
601 an increase in C storage by high-latitude ecosystems in a warming, high-CO₂ climate.
602 Baseline (1961-1990) NPPs simulated by RCA-GUESS across the Arctic are within the range
603 of variability of observations (Fig 5a). Although the present study does not include N
604 limitation, the simulated increase in ecosystem C storage across the Arctic may be realistic.
605 How nutrient cycling effects may impact biogeophysical land-climate interaction remains
606 unclear and needs further investigation.

607 **5 Conclusion**

608 Our simulations with a regional ESM suggest that in the present climate, Arctic ecosystems
609 are acting as a weak C sink, consistent with findings from some other process-based models
610 and inversion studies. Under an RCP 8.5 future climate scenario, an increased C uptake rate is
611 projected until the 2060s-2070s, after which C uptake declines as increased soil respiration
612 and biomass burning outpaces further increases in vegetation net primary productivity.
613 Biogeophysical effects from climate-vegetation interactions, leading to an earlier, longer
614 growing-season and milder peak temperatures in summer, enhance the initial increase in the C
615 sink by accentuating NPP and postponing the peak C uptake rate by some 15 years. Integrated
616 over the 21st century, the additional C sinks arising from biogeophysical feedbacks are some
617 8.5 Gt C, or 22% of the total C sink, of which 83.5% is located in areas currently classified as
618 Arctic tundra. The net effects of biogeophysical feedbacks to the regional climate result from
619 two opposing feedback mechanisms, namely the albedo feedback and the evapotranspiration
620 feedback. The former dominates in the winter and spring seasons, amplifying the near-
621 surface warming by up to 1.35  C in spring, while the latter dominates in summer, resulting in
622 an evaporative cooling of up to 0.81  C. Such feedbacks stimulate vegetation growth with an
623 earlier onset of the growing-season, leading to compositional changes in woody plants and
624 vegetation redistribution.

625 **Acknowledgements**

626 The model simulations were carried out at the National Supercomputer Centre (NSC) in
627 Linköping, Sweden. The study is funded by the Swedish Research Council FORMAS within
628 the project Advanced Simulation of Arctic Climate and Impact on Northern Regions
629 (ADSIMNOR). The authors would like to thank the Rossby Centre at the Swedish
630 Meteorological and Hydrological Institute (SMHI) for coordinating this project, and thank
631 Prof. A. David McGuire and Dr. Anders Ahlström for providing additional data to evaluate
632 our results. The study is a contribution to the strategic research areas Modelling the Regional
633 and Global Earth System (MERGE) and Biodiversity and Ecosystem Services in a Changing
634 Climate (BECC), the Lund University Centre for the study of Climate and Carbon Cycle
635 (LUCCI) and the Nordic Centre of Excellence DEFROST.
636

637 **References**

- 638 Ahlström, A., Miller, P.A., and Smith, B.: Too early to infer a global NPP decline since 2000.
639 *Geophysical Research Letters*, 39, L15403, DOI: 10.1029/2012GL052336, 2012a.
- 640 Ahlström, A., Schurgers, G., Arneeth, A., and Smith, B.: Robustness and uncertainty in
641 terrestrial ecosystem carbon response to CMIP5 climate change projections, *Environ. Res.
642 Lett.*, 7, 044008, doi:10.1088/1748-9326/7/4/044008, 2012b.
- 643 Bathiany, S., Claussen, M., Brovkin, V., Raddatz, T., and Gayler, V.: Combined
644 biogeophysical and biogeochemical effects of large-scale forest cover changes in the MPI
645 earth system model, *Biogeosciences*, 7, 1383-1399, doi:10.5194/bg-7-1383-2010, 2010.
- 646 Beck, P. S. A., and Goetz, S. J.: Satellite observations of high northern latitude vegetation
647 productivity changes between 1982 and 2008: ecological variability and regional differences,
648 *Environ. Res. Lett.*, 6, 045501, doi:10.1088/1748-9326/6/4/045501, 2011.
- 649 Betts, R. A.: Offset of the potential carbon sink from boreal forestation by decreases in
650 surface albedo, *Nature*, 408, 187-190, doi:10.1038/35041545, 2000.
- 651 Blok, D., Heijmans, M. M. P. D., Schaepman-Strub, G., Kononov, A. V., Maximov, T. C.,
652 and Berendse, F.: Shrub expansion may reduce summer permafrost thaw in Siberian tundra,
653 *Glob. Change Biol.*, 16, 1296–1305, 2010.
- 654 Bonan, G. B.: Forests and Climate Change: Forcings, Feedbacks, and the Climate Benefits of
655 Forests, *Science*, 320, 1444-1449, doi:10.1126/science.1155121, 2008.
- 656 Bonfils, C. J. W., Phillips, T. J., Lawrence, D. M., Cameron-Smith, P., Riley, W. J., and
657 Subin, Z. M.: On the influence of shrub height and expansion on northern high latitude
658 climate, *Environ. Res. Lett.*, 7, 015503, doi:10.1088/1748-9326/7/1/015503, 2012.
- 659 Brovkin, V., Claussen, M., Driesschaert, E., Fichefet, T., Kicklighter, D., Loutre, M. F.,
660 Matthews, H. D., Ramankutty, N., Schaeffer, M., and Sokolov, A.: Biogeophysical effects of
661 historical land cover changes simulated by six Earth system models of intermediate
662 complexity, *Clim. Dynam.*, 26, 587-600, doi:10.1007/s00382-005-0092-6, 2006.
- 663 Brovkin, V., Boysen, L., Raddatz, T., Gayler, V., Loew, A., and Claussen, M.: Evaluation of
664 vegetation cover and land-surface albedo in MPI-ESM CMIP5 simulations, *Journal of
665 Advances in Modeling Earth Systems*, 5, 48-57, doi:10.1029/2012MS000169, 2013.

666 Chapin, F. S., Sturm, M., Serreze, M. C., McFadden, J. P., Key, J. R., Lloyd, A. H., McGuire,
667 A. D., Rupp, T. S., Lynch, A. H., Schimel, J. P., Beringer, J., Chapman, W. L., Epstein, H. E.,
668 Euskirchen, E. S., Hinzman, L. D., Jia, G., Ping, C.-L., Tape, K. D., Thompson, C. D. C.,
669 Walker, D. A., and Welker, J. M.: Role of Land-Surface Changes in Arctic Summer
670 Warming, *Science*, 310, 657-660, doi: 10.1126/science.1117368, 2005.

671 Cox, P. M., Betts, R. A., Jones, C. D., Spall, S. A., and Totterdell, I. J.: Acceleration of global
672 warming due to carbon-cycle feedbacks in a coupled climate model, *Nature*, 408, 184-187,
673 doi:10.1038/35041539, 2000.

674 Denissenko, E. A., Brovkin, V., and Cramer, W.: NPP Multi-Biome: PIK Data for Northern
675 Eurasia, 1940-1988 (Based on Bazilevich), Data set. Available on-line [<http://daac.ornl.gov>]
676 from Oak Ridge National Laboratory Distributed Active Archive Center, Oak Ridge,
677 Tennessee, USA, doi:10.3334/ORNLDAAC/575, 2013.

678 Elmendorf, S. C., Henry, G. H. R., Hollister, R. D., Bjork, R. G., Boulanger-Lapointe, N.,
679 Cooper, E. J., Cornelissen, J. H. C., Day, T. A., Dorrepaal, E., Elumeeva, T. G., Gill, M.,
680 Gould, W. A., Harte, J., Hik, D. S., Hofgaard, A., Johnson, D. R., Johnstone, J. F., Jonsdottir,
681 I. S., Jorgenson, J. C., Klanderud, K., Klein, J. A., Koh, S., Kudo, G., Lara, M., Levesque, E.,
682 Magnusson, B., May, J. L., Mercado-Diaz, J. A., Michelsen, A., Molau, U., Myers-Smith, I.
683 H., Oberbauer, S. F., Onipchenko, V. G., Rixen, C., Martin Schmidt, N., Shaver, G. R.,
684 Spasojevic, M. J., orhallsdottir, o. E., Tolvanen, A., Troxler, T., Tweedie, C. E., Villareal, S.,
685 Wahren, C.-H., Walker, X., Webber, P. J., Welker, J. M., and Wipf, S.: Plot-scale evidence of
686 tundra vegetation change and links to recent summer warming, *Nature Clim. Change*, 2, 453-
687 457, doi:10.1038/nclimate1465, 2012.

688 Euskirchen, E. S., McGuire, A. D., Rupp, T. S., Chapin III, F. S., and Walsh J. E.: Projected
689 changes in atmospheric heating due to changes in fire disturbance and the snow season in the
690 western Arctic, 2003–2100, *J. Geophys. Res.*, 114, G04022, doi:10.1029/2009JG001095,
691 2009.

692 Falloon, P. D., Dankers, R., Betts, R. A., Jones, C. D., Booth, B. B. B., and Lambert, F. H.:
693 Role of vegetation change in future climate under the A1B scenario and a climate stabilisation
694 scenario, using the HadCM3C Earth system model, *Biogeosciences*, 9, 4739-4756,
695 doi:10.5194/bg-9-4739-2012, 2012.

696 Gerten, D., Schaphoff, S., Haberlandt, U., Lucht, W., Sitch, S.: Terrestrial vegetation and
697 water balance—hydrological evaluation of a dynamic global vegetation model, *Journal of*
698 *Hydrology*, 286, 249-270, doi:10.1016/j.jhydrol.2003.09.029, 2004.

699 Goll, D. S., Brovkin, V., Parida, B. R., Reick, C. H., Kattge, J., Reich, P. B.,
700 van Bodegom, P. M., and Niinemets, Ü.: Nutrient limitation reduces land carbon uptake in
701 simulations with a model of combined carbon, nitrogen and phosphorus cycling,
702 *Biogeosciences Discuss.*, 9, 3173-3232, doi:10.5194/bgd-9-3173-2012, 2012.

703 Hayes, D. J., Turner, D. P., Stinson, G., McGuire, A. D., Wei, Y., West, T. O., Heath, L. S.,
704 de Jong, B., McConkey, B. G., Birdsey, R. A., Kurz, W. A., Jacobson, A. R., Huntzinger, D.
705 N., Pan, Y., Post, W. M., and Cook, R. B.: Reconciling estimates of the contemporary North
706 American carbon balance among terrestrial biosphere models, atmospheric inversions, and a
707 new approach for estimating net ecosystem exchange from inventory-based data, *Glob.*
708 *Change Biol.*, 18, 1282-1299, 2012.

709 Hayes, D. J., McGuire, A. D., Kicklighter, D. W., Gurney, K. R., Burnside, T. J., and Melillo,
710 J. M.: Is the northern high-latitude land-based CO₂ sink weakening? *Global Biogeochem.*
711 *Cy.*, 25, GB3018, doi:10.1029/2010GB003813, 2011.

712 Hazeleger, W., Severijns, C., Semmler, T., Ștefănescu, S., Yang, S., Wang, X., Wyser, K.,
713 Dutra, E., Baldasano, J. M., Bintanja, R., Bougeault, P., Caballero, R., Ekman, A. M. L.,
714 Christensen, J. H., van den Hurk, B., Jimenez, P., Jones, C., Källberg, P., Koenigk, T.,
715 McGrath, R., Miranda, P., van Noije, T., Palmer, T., Parodi, J. A., Schmith, T., Selten, F.,
716 Storelvmo, T., Sterl, A., Tapamo, H., Vancoppenolle, M., Viterbo, P., and Willmott, U.: EC-
717 Earth: a seamless earth-system prediction approach in action, *Bull. Amer. Meteor. Soc.*, 91,
718 1357–1363, doi: 10.1175/2010BAMS2877.1, 2010.

719 Hazelegger, W., Wang, X., Severijns, C., Ștefănescu, S., Bintanja, R., Sterl, A., Wyser, K.,
720 Semmler, T., Yang, S., van den Hurk, B., van Noije, T., van der Linden, E., van der Wiel, K.:
721 EC-Earth V2.2: description and validation of a new seamless Earth system prediction model.
722 *Clim. Dyn.*, 39, 2611-2629, 2012.

723 Hickler, T., Vohland, K., Feehan, J., Miller, P. A., Smith, B., Costa, L., Giesecke, T.,
724 Fronzek, S., Carter, T. R., Cramer, W., Kühn, I., and Sykes, M. T.: Projecting the future
725 distribution of European potential natural vegetation zones with a generalized, tree species-

726 based dynamic vegetation model, *Global Ecol. Biogeogr.*, 21, 50-63, doi:10.1111/j.1466-
727 8238.2010.00613.x, 2012.

728 Jiang, Y., Zhuang, Q., Schaphoff, S., Sitch, S., Sokolov, A., Kicklighter, D., and Melillo, J.:
729 Uncertainty analysis of vegetation distribution in the northern high latitudes during the 21st
730 century with a dynamic vegetation model, *Ecology and Evolution*, 2, 593-614,
731 doi:10.1002/ece3.85, 2012.

732 Kasurinen, V., Alfredsen, K., Kolari, P., Mammarella, I., Alekseychik, P., Rinne, J., Vesala,
733 T., Bernier, P., Boike, J., Langer, M., Belelli Marchesini, L., van Huissteden, K., Dolman, H.,
734 Sachs, T., Ohta, T., Varlagin, A., Rocha, A., Arain, A., Oechel, W., Lund, M., Grelle, A.,
735 Lindroth, A., Black, A., Aurela, M., Laurila, T., Lohila, A. and Berninger, F.: Latent heat
736 exchange in the boreal and arctic biomes, *Global Change Biology*, doi: 10.1111/gcb.12640,
737 2014.

738 Keuper, F., Parmentier, F. J., Blok, D., Bodegom, P., Dorrepaal, E., Hal, J., Logtestijn, R. P.,
739 and Aerts, R.: Tundra in the rain: differential vegetation responses to three years of
740 experimentally doubled summer precipitation in siberian shrub and swedish bog tundra,
741 *Ambio*, 41, 269-280, doi:10.1007/s13280-012-0305-2, 2012.

742 Kimball, J. S., Jones, L. A., Zhang, K., Heinsch, F. A., McDonald, K. C., and Oechel, W. C.:
743 A satellite approach to estimate land-atmosphere CO₂ exchange for Boreal and Arctic biomes
744 using MODIS and AMSR-E, *IEEE T. Geosci. Remote*, 47, 569–587,
745 doi:10.1109/TGRS.2008.2003248, 2009.

746 Koenigk, T., Brodeau, L., Graversen, R., Karlsson, J., Svensson, G., Tjernström, M., Willén,
747 U., and Wyser, K.: Arctic climate change in 21st century CMIP5 simulations with EC-Earth,
748 *Clim. Dynam.*, 40, 2719-2743, doi:10.1007/s00382-012-1505-y, 2013.

749 Koca, D., Smith, B., Sykes M. T.: Modelling Regional Climate Change Effects On Potential
750 Natural Ecosystems in Sweden, *Climatic Change*, 78, 381-406, doi:10.1007/s10584-005-
751 9030-1, 2006.

752 Koven, C. D., Friedlingstein, P., Ciais, P., Khvorostyanov, D., Krinner, G., and Tarnocai, C.:
753 On the formation of high-latitude soil carbon stocks: Effects of cryoturbation and insulation
754 by organic matter in a land surface model, *Geophys. Res. Lett.*, 36, L21501,
755 doi:10.1029/2009GL040150, 2009.

756 Koven, C. D., Ringeval, B., Friedlingstein, P., Ciais, P., Cadule, P., Khvorostyanov, D.,
757 Krinner, G., and Tarnocai, C.: Permafrost carbon-climate feedbacks accelerate global
758 warming, *P. Natl. Acad. Sci.*, 108, 14769–14774, 2011.

759 Kueppers, L. M., Snyder, M. A., Sloan L. C., Zavaleta, E. S., and Fulfrost. B.: Modelled
760 regional climate change and California endemic oak ranges, *P. Natl. Acad. Sci.*, 102 (45),
761 16281-16286, 2005.

762 Loranty, M. M., Berner, L. T., Goetz, S. J., Jin, Y., and Randerson, J. T.: Vegetation controls
763 on northern high latitude snow-albedo feedback: observations and CMIP5 model predictions,
764 *Glob. Change Biol.*, 20, 594-606, doi:10.1111/gcb.12391, 2014.

765 Loveland, T. R., Reed B. C., Brown J. F., Ohlen D. O., Zhu Z., Yang L., and Merchant J. W.:
766 Development of a global land cover characteristics database and IGBP DISCover from 1 km
767 AVHRR data, *International Journal of Remote Sensing*, 21, 6-7, 1303-1330,
768 doi:10.1080/014311600210191, 2000.

769 Lawrence, D. M., and Swenson S. C.: Permafrost response to increasing Arctic shrub
770 abundance depends on the relative influence of shrubs on local soil cooling versus large-scale
771 climate warming, *Environ. Res. Lett.*, 6, 045504, doi:10.1088/1748-9326/6/4/045504, 2011.

772 MacDougall, A. H., Avis C. A., and Weaver A. J.: Significant contribution to climate
773 warming from the permafrost carbon feedback, *Nat. Geosci.*, 5, 719–721,
774 doi:10.1038/ngeo1573, 2012.

775 Matthes, H., Rinke, A., Miller, P., Kuhry, P., Dethloff, K., and Wolf, A.: Sensitivity of high-
776 resolution Arctic regional climate model projections to different implementations of land
777 surface processes, *Climatic Change*, 111, 197-214, doi:10.1007/s10584-011-0138-1, 2011.

778 McGuire, A. D., Hayes, D. J., Kicklighter, D. W., Manizza, M., Zhuang, Q., Chen, M.,
779 Follows, M. J., Gurney, K. R., McClelland, J.W., Melillo, J.M., Peterson, B. J., and Prinn, R.:
780 An analysis of the carbon balance of the Arctic Basin from 1997 to 2006, *Tellus B*, 62, 455–
781 474, doi:10.1111/j.1600-0889.2010.00497.x, 2010.

782 McGuire, A. D., Christensen, T. R., Hayes, D., Heroult, A., Euskirchen, E., Yi, Y., Kimball,
783 J. S., Koven, C., Lafleur, P., Miller, P. A., Oechel, W., Peylin, P., and Williams, M.: An
784 assessment of the carbon balance of arctic tundra: comparisons among observations, process
785 models, and atmospheric inversions, *Biogeosciences*, 9, 3185-3204, doi:10.5194/bg-9-3185-
786 2012, 2012.

787 Miller, P. A., and Smith, B.: Modelling Tundra Vegetation Response to Recent Arctic
788 Warming, *Ambio*, 41, 281-291, doi:10.1007/s13280-012-0306-1, 2012.

789 Mitchell, T. D., and Jones, P. D.: An improved method of constructing a database of monthly
790 climate observations and associated high-resolution grids, *International Journal of*
791 *Climatology*, 25, 693-712, doi:10.1002/joc.1181, 2005.

792 Monson, R. K., Lipson, D. L., Burns, S. P., Turnipseed, A. A., Delany, A. C., Williams M.
793 W., Schmidt S. K.: Winter forest soil respiration controlled by climate and microbial
794 community composition, *Nature*, 439, 711-714, doi:10.1038/nature04555, 2006.

795 Morales, P., Sykes, M. T., Prentice, I. C., Smith, P., Smith, B., Bugmann, H., Zierl, B.,
796 Friedlingstein, P., Viovy, N., Sabaté S., Sánchez, A., Pla, E., Gracia, C. A., Sitch, S., Arneth,
797 A. and Ogee, J.: Comparing and evaluating process-based ecosystem model predictions of
798 carbon and water fluxes in major European forest biomes, *Global Change Biology*, 11: 2211–
799 2233, doi: 10.1111/j.1365-2486.2005.01036.x, 2005.

800 Morales, P., Hickler, T., Rowell, D. P., Smith, B. and Sykes, M. T.: Changes in European
801 ecosystem productivity and carbon balance driven by regional climate model output, *Global*
802 *Change Biology*, 13, 108–122, doi: 10.1111/j.1365-2486.2006.01289.x, 2007.

803 Moss, R. H., Edmonds, J. A., Hibbard, K. A., Manning, M. R., Rose, S. K., van Vuuren, D.
804 P., Carter, T. R., Emori, S., Kainuma, M., Kram, T., Meehl, G. A., Mitchell, J. F. B.,
805 Nakicenovic, N., Riahi, K., Smith, S. J., Stouffer, R. J., Thomson, A. M., Weyant, J. P., and
806 Wilbanks, T. J.: The next generation of scenarios for climate change research and assessment,
807 *Nature*, 463, 747-756, doi:10.1038/nature08823, 2010.

808 Olson, R. J., Scurlock, J. M. O., Prince, S. D., Zheng, D. L., and Johnson, K. R (eds.): NPP
809 Multi-Biome: NPP and Driver Data for Ecosystem Model Data Intercomparison, R2. Data set.
810 Available on-line [<http://daac.ornl.gov>] from Oak Ridge National Laboratory Distributed
811 Active Archive Center, Oak Ridge, Tennessee, USA, doi:10.3334/ORNLDAAC/615, 2013a.

812 Olson, R. J., Scurlock, J. M. O., Prince, S. D., Zheng, D. L., and Johnson, K. R (eds.): NPP
813 Multi-Biome: Global Primary Production Data Initiative Products, R2. Data set. Available on-
814 line [<http://daac.ornl.gov>] from the Oak Ridge National Laboratory Distributed Active
815 Archive Center, Oak Ridge, Tennessee, USA, doi:10.3334/ORNLDAAC/617, 2013b.

816 Oechel, W. C., Hastings, S. J., Vourlirts, G., Jenkins, M., Riechers, G., and Grulke, N.:
817 Recent change of Arctic tundra ecosystems from a net carbon dioxide sink to a source,
818 *Nature*, 361, 520-523, doi:10.1038/361520a0, 1993.

819 Pan, Y., Birdsey, R. A., Fang, J., Houghton, R., Kauppi, P. E., Kurz, W. A., Phillips, O. L.,
820 Shvidenko, A., Lewis, S. L., Canadell, J. G., Ciais, P., Jackson, R. B., Pacala, S. W.,
821 McGuire, A. D., Piao, S., Rautiainen, A., Sitch, S., and Hayes, D.: A Large and Persistent
822 Carbon Sink in the World's Forests, *Science*, 333, 988-993, doi:10.1126/science.1201609,
823 2011.

824 Peylin, P., Law, R. M., Gurney, K. R., Chevallier, F., Jacobson, A. R., Maki, T., Niwa, Y.,
825 Patra, P. K., Peters, W., Rayner, P. J., Rödenbeck, C., van der Laan-Luijkx, I. T., and Zhang,
826 X.: Global atmospheric carbon budget: results from an ensemble of atmospheric CO₂
827 inversions, *Biogeosciences*, 10, 6699-6720, doi:10.5194/bg-10-6699-2013, 2013.

828 Piao, S., Fang, J., Zhou, L., Ciais, P., and Zhu, B.: Variations in satellite-derived phenology in
829 China's temperate vegetation, *Glob. Change Biol.*, 12, 672-685, doi:10.1111/j.1365-
830 2486.2006.01123.x, 2006.

831 Poulter, B., Frank, D. C., Hodson, E. L., and Zimmermann, N. E.: Impacts of land cover and
832 climate data selection on understanding terrestrial carbon dynamics and the CO₂ airborne
833 fraction, *Biogeosciences*, 8, 2027-2036, doi:10.5194/bg-8-2027-2011, 2011.

834 Qian, H., Joseph, R., and Zeng, N.: Enhanced terrestrial carbon uptake in the Northern High
835 Latitudes in the 21st century from the Coupled Carbon Cycle Climate Model Intercomparison
836 Project model projections, *Glob. Change Biol.*, 16, 641-656, doi:10.1111/j.1365-
837 2486.2009.01989.x, 2010.

838 Quillet, A., Peng, C., and Garneau, M.: Toward dynamic global vegetation models for
839 simulating vegetation–climate interactions and feedbacks: recent developments, limitations,
840 and future challenges, *Environmental Reviews*, 18, 333-353, doi:10.1139/A10-016, 2010.

841 Ramankutty, N., and Foley, J. A.: ISLSCP II Potential Natural Vegetation Cover. In Hall,
842 Forest G., Collatz, G., Meeson, B., Los, S., Brown de Colstoun, E., and Landis D., (eds.):
843 ISLSCP Initiative II Collection. Data set. Available on-line [http://daac.ornl.gov/] from Oak
844 Ridge National Laboratory Distributed Active Archive Center, Oak Ridge, Tennessee, USA,
845 doi:10.3334/ORNLDAAAC/961, 2010.

846 Rietkerk, M., Brovkin, V., van Bodegom, P. M., Claussen, M., Dekker, S. C., Dijkstra, H. A.,
847 Goryachkin, S. V., Kabat, P., van Nes, E. H., Neutel, A.-M., Nicholson, S. E., Nobre, C.,
848 Petoukhov, V., Provenzale, A., Scheffer, M., and Seneviratne, S. I.: Local ecosystem
849 feedbacks and critical transitions in the climate, *Ecological Complexity*, 8, 223-228,
850 doi:10.1016/j.ecocom.2011.03.001, 2011.

851 Ruckstuhl, K. E., Johnson, E., and Miyanishi, K.: Introduction. The boreal forest and global
852 change, *Philosophical Transactions of the Royal Society of Biological Sciences*, 363, 2245–
853 2249, doi:10.1098/rstb.2007.2196, 2008.

854 Rummukainen, M.: State-of-the-art with regional climate models, *Wiley Interdisciplinary*
855 *Reviews: Climate Change*, 1, 82-96, doi:10.1002/wcc.8, 2010.

856 Samuelsson, P., Gollvik, S., and Ullerstig, A.: The land-surface scheme of the Rossby Centre
857 regional atmospheric climate model (RCA3), *Reports Meteorol. Climatol.*, 12, 38, 2006.

858 Samuelsson, P., Jones, C. G., WillÉN, U., Ullerstig, A., Gollvik, S., Hansson, U. L. F.,
859 Jansson, C., KjellstrÖM, E., Nikulin, G., and Wyser, K.: The Rossby Centre Regional Climate
860 model RCA3: model description and performance, *Tellus A*, 63, 4-23, doi:10.1111/j.1600-
861 0870.2010.00478.x, 2011.

862 Seneviratne, S. I., Corti, T., Davin, E. L., Hirschi, M., Jaeger, E. B., Lehner, I., Orlowsky, B.,
863 and Teuling, A. J.: Investigating soil moisture–climate interactions in a changing climate: A
864 review, *Earth-Science Reviews*, 99, 125-161, doi:10.1016/j.earscirev.2010.02.004, 2010.

865 Schuur, E. A. G., Abbott, B. W., Bowden, W. B., Brovkin, V., Camill, P., Canadell, J. G.,
866 Chanton, J. P., Chapin III, F. S., Christensen, T. R., Ciais, P., Crosby, B. T., Czimczik, C. I.,
867 Grosse, G., Harden, J., Hayes, D. J., Hugelius, G., Jastrow, J. D., Jones, J. B., Kleinen, T.,
868 Koven, C. D., Krinner, G., Kuhry, P., Lawrence, D. M., McGuire, A. D., Natali, S. M.,
869 O'Donnell, J. A., Ping, C. L., Riley, W. J., Rinke, A., Romanovsky, V. E., Sannel, A. B. K.,
870 Sch ädel, C., Schaefer, K., Sky, J., Subin, Z. M., Tarnocai, C., Turetsky, M. R., Waldrop, M.
871 P., Walter Anthony, K. M., Wickland, K. P., Wilson, C. J., and Zimov, S. A.: Expert
872 assessment of vulnerability of permafrost carbon to climate change, *Climatic Change*, 119,
873 359–374, 2013.

874 Shuman, J. K., Shugart, H. H., and O'Halloran, T. L.: Sensitivity of Siberian larch forests to
875 climate change, *Glob. Change Biol.*, 17, 2370–84, 2011.

876 Sitch, S., Smith, B., Prentice, I. C., Arneeth, A., Bondeau, A., Cramer, W., Kaplan, J. O.,
877 Levis, S., Lucht, W., Sykes, M. T., Thonicke, K., and Venevsky, S.: Evaluation of ecosystem
878 dynamics, plant geography and terrestrial carbon cycling in the LPJ dynamic global
879 vegetation model, *Glob. Change Biol.*, doi:10.1046/j.1365-2486.2003.00569.x, 2003.

880 Sitch, S., McGuire, A. D., Kimball, J., Gedney, N., Gamon, J., Engstrom, R., Wolf, A.,
881 Zhuang, Q., Clein, J., and McDonald, K. C.: Assessing the carbon balance of circumpolar
882 arctic tundra using remote sensing and process modeling, *Ecol. Appl.*, 17, 213-234, 2007.

883 Sitch, S., Huntingford, C., Gedney, N., Levy, P. E., Lomas, M., Piao, S. L., Betts, R., Ciais,
884 P., Cox, P., Friedlingstein, P., Jones, C. D., Prentice, I. C. and Woodward, F. I.: Evaluation of
885 the terrestrial carbon cycle, future plant geography and climate carbon cycle feedbacks using
886 five dynamic global vegetation models (DGVMs), *Glob. Change Biol.*, 14,
887 doi:10.1111/j.1365-2486.2008.01626.x, 2008.

888 Smith, B., Prentice, I. C., and Sykes, M. T.: Representation of vegetation dynamics in the
889 modelling of terrestrial ecosystems: comparing two contrasting approaches within European
890 climate space, *Global Ecol. Biogeogr.*, 10, 621-637, doi:10.1046/j.1466-822X.2001.t01-1-
891 00256.x, 2001.

892 Smith, B., Samuelsson, P., Wramneby, A., and Rummukainen, M.: A model of the coupled
893 dynamics of climate, vegetation and terrestrial ecosystem biogeochemistry for regional
894 applications, *Tellus: Series A*, 63, 87-106, doi:10.1111/j.1600-0870.2010.00477.x, 2011.

895 Smith, B., W  rlind, D., Arneeth, A., Hickler, T., Leadley, P., Siltberg, J., and Zaehle, S.:
896 Implications of incorporating N cycling and N limitations on primary production in an
897 individual-based dynamic vegetation model, *Biogeosciences*, 11, 2027-2054, 2014.

898 Swann, A. L., Fung, I. Y., Levis, S., Bonan, G., and Doney, S.: Changes in Arctic vegetation
899 induce high-latitude warming through the greenhouse effect. *P. Natl. Acad. Sci. USA*, 107,
900 1295–1300, doi:10.1073/pnas.0913846107, 2010.

901 Tape, K. E. N., Sturm, M., and Racine, C.: The evidence for shrub expansion in Northern
902 Alaska and the Pan-Arctic, *Glob. Change Biol.*, 12, 686-702, doi:10.1111/j.1365-
903 2486.2006.01128.x, 2006.

904 Valentini, R., Matteucci, G., Dolman, A. J., Schulze, E. D., Rebmann, C., Moors, E. J.,
905 Granier, A., Gross, P., Jensen, N. O., Pilegaard, K., Lindroth, A., Grelle, A., Bernhofer, C.,
906 Grunwald, T., Aubinet, M., Ceulemans, R., Kowalski, A. S., Vesala, T., Rannik, U.,

907 Berbigier, P., Loustau, D., Gumundsson, J., Thorgeirsson, H., Ibrom, A., Morgenstern, K.,
908 Clement, R., Moncrieff, J., Montagnani, L., Minerbi, S., and Jarvis, P. G.: Respiration as the
909 main determinant of carbon balance in European forests, *Nature*, 404, 861-865,
910 doi:10.1038/35009084, 2000.

911 Wania, R., Ross, I., and Prentice, I. C.: Integrating peatlands and permafrost into a dynamic
912 global vegetation model: I. Evaluation and sensitivity of physical land surface processes,
913 *Global Biogeochem. Cy.*, 23, GB3014, doi:10.1029/2008GB003412, 2009a.

914 Wania, R., Ross, I., and Prentice, I. C.: Integrating peatlands and permafrost into a dynamic
915 global vegetation model: II. Evaluation and sensitivity of vegetation and carbon cycle
916 processes, *Global Biogeochem. Cy.*, 23, GB015, doi:10.1029/2008GB003413, 2009b.

917 Wania, R., Ross, I., and Prentice, I. C.: Implementation and evaluation of a new methane
918 model within a dynamic global vegetation model: LPJ-WHyMe v1.3.1, *Geosci. Model Dev.*,
919 3, 565–584, doi:10.5194/gmd-3-565-2010, 2010.

920 Wårlind, D., Smith, B., Hickler, T., and Arneeth, A.: Nitrogen feedbacks increase future
921 terrestrial ecosystem carbon uptake in an individual-based dynamic vegetation model,
922 *Biogeosciences Discuss.*, 11, 151-185, 2014.

923 Willmott, C. J., and Matsuura, K. 1995.: Smart interpolation of annually averaged air
924 temperature in the United States, *J. Appl. Met.*, 34, 2577–2586

925 Wolf, A., Callaghan, T., and Larson, K.: Future changes in vegetation and ecosystem function
926 of the Barents Region, *Climatic Change*, 87, 51-73, doi:10.1007/s10584-007-9342-4, 2008.

927 Wramneby, A., Smith, B., and Samuelsson, P.: Hot spots of vegetation-climate feedbacks
928 under future greenhouse forcing in Europe, *J. Geophys. Res.*, 115, D21119,
929 doi:10.1029/2010jd014307, 2010.

930 Zaehle, S. and Dalmonech, D.: Carbon-nitrogen interactions on land at global scales:
931 understanding in modelling climate biosphere feedbacks, *Current Opinions in Environmental*
932 *Sustainability*, 3, 311-320, 2011.

933 Zaehle, S., Medlyn, B. E., De Kauwe, M. G., Walker, A. P., Dietze, M. C., Hickler, T., Luo,
934 Y., Wang, Y.-P., El-Masri, B., Thornton, P., Jain, A., Wang, S., Warlind, D., Weng, E.,
935 Parton, W., Iversen, C. M., Gallet-Budynek, A., McCarthy, H., Finzi, A., Hanson, P. J.,
936 Prentice, I. C., Oren, R., and Norby, R. J.: Evaluation of 11 terrestrial carbon–nitrogen cycle

937 models against observations from two temperate Free-Air CO₂ Enrichment studies, *New*
938 *Phytologist*, doi:10.1111/nph.12697, 2014.

939 Zhang, W., Miller, P. A., Smith, B., Wania, R., Koenigk, T., and Döscher, R.: Tundra
940 shrubification and tree-line advance amplify arctic climate warming: results from an
941 individual-based dynamic vegetation model, *Environ. Res. Lett.*, 8, 034023,
942 doi:10.1088/1748-9326/8/3/034023, 2013a.

943 Zhang, Q., Wang, Y. P., Matear R. J., Pitman, A. J., and Dai Y. J.: Nitrogen and phosphorous
944 limitations significantly reduce future allowable CO₂ emissions, *Geophys. Res. Lett.*, 41,
945 doi:10.1002/2013GL058352, 2013b.

946 Zheng, D. L., Prince, S. D., and Wright, R., NPP Multi-Biome: Gridded Estimates for
947 Selected Regions Worldwide, 1954-1998, R3. Data set. Available on-line
948 [<http://daac.ornl.gov>] from the Oak Ridge National Laboratory Distributed Active Archive
949 Center, Oak Ridge, Tennessee, USA, doi:10.3334/ORNLDAAAC/614, 2013.

950

951

952

953

954

955

956

957

958

959

960

961

962 **Figures and Tables**

963 **Table 1.** Mean carbon budget of Arctic tundra simulated by process-based models, inversion
964 models and RCA-GUESS for the period 1990-2006.

Model	C flux (g C m ⁻² yr ⁻¹)					The slope of the linear trend (-)
	NPP	RH	NEP	FIRE	NEE	
LPJ-GUESS WhyMe	-130	106	-24	1	-23	-0.53
ORCHIDEE	-361	330	-31	-	-31	-0.63
TEM6	-107	97	-10	8	-2	0.25
TCF	-181	183	-2	-	-2	-0.62
The ensemble mean of inversion models	-	-	-	-	-13	0.2
RCA-GUESS	-266	233	-33	15	-18	-0.35
RCA-GUESS nf. ¹	-268	234	-34	15	-19	0.24

965 ¹nf.: the non-feedback run.

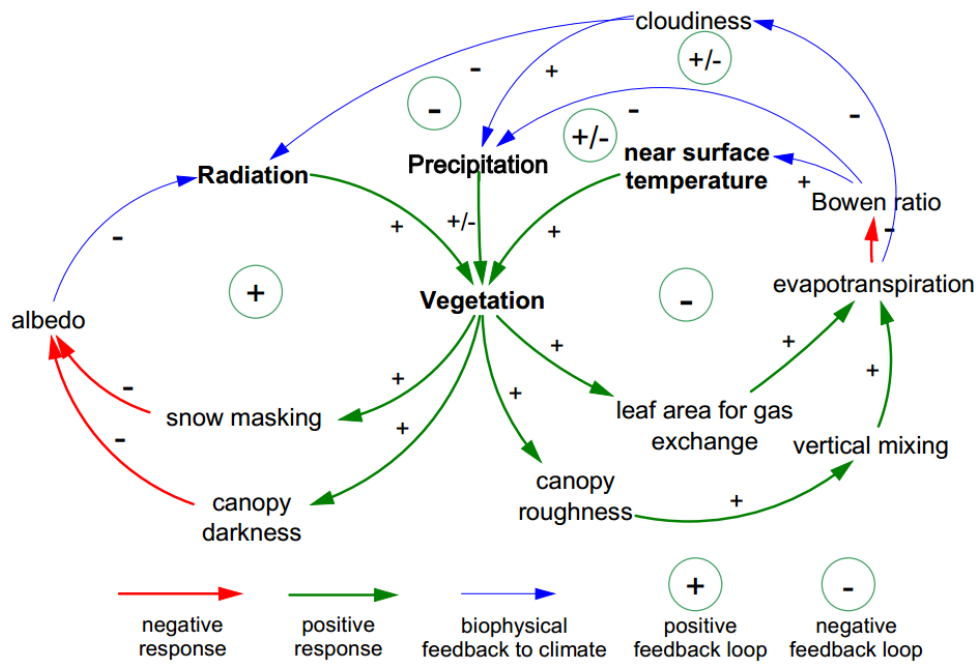
966 **Table 2.** Carbon budget of the Arctic tundra and CORDEX-Arctic domains simulated by
967 RCA-GUESS for the period 1990-2100.

Domains	Accumulative C flux (Gt C)					C stores (Gt C)		
	NPP	RH	NEP	FIRE	NEE	VegC	LittC	SoilC
Arctic tundra fb. ¹	-302.1	257.7	-44.4	8.8	-35.6	33.9	0.5	1.2
Arctic tundra nf. ²	-288.9	251.8	-37.1	8.6	-28.5	29.6	-1.3	0.2
Arctic tundra diff. ³	-13.2	5.9	-7.3	0.2	-7.1	4.3	1.8	1
CORDEX-Arctic fb.	-541.2	474.5	-66.7	28	-38.7	46.9	-1.8	-6.4
CORDEX-Arctic nf.	-525.3	467.1	-58.2	28	-30.2	42.1	-4	-7.9
CORDEX-Arctic diff.	-15.9	7.4	-8.5	0	-8.5	4.8	2.2	1.5

968 ¹fb.: the feedback run; ²nf.: the non-feedback run; ³diff.: the feedback run minus the non-feedback run. Note:
969 negative values in C flux mean C uptake, but negative values in C stores mean absolute reductions of C stores.

970

971



972

973 **Fig. 1.** Diagram of climate-vegetation interaction feedback loops that comprise positive
 974 responses (green), negative responses (red) arising from vegetation change and consequent
 975 biogeophysical feedbacks to climate (blue).

976

977

978

979

980

981

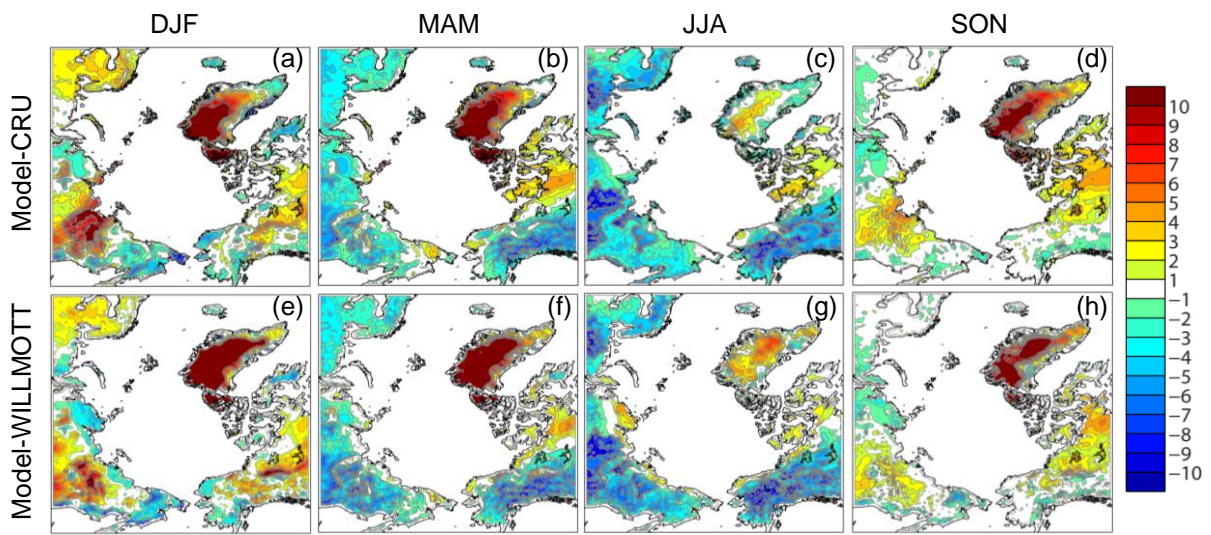
982

983

984

985

986



987

988 **Fig. 2.** The mean seasonal 2m temperature anomalies (°C) relative to the CRU and
 989 WILLMOT datasets for the period 1961-1990. (a, e) Winter, December to February (DJF). (b,
 990 f) Spring, March to May (MAM). (c, g) Summer, June to August (JJA). (d, h) Autumn,
 991 September to November (SON).

992

993

994

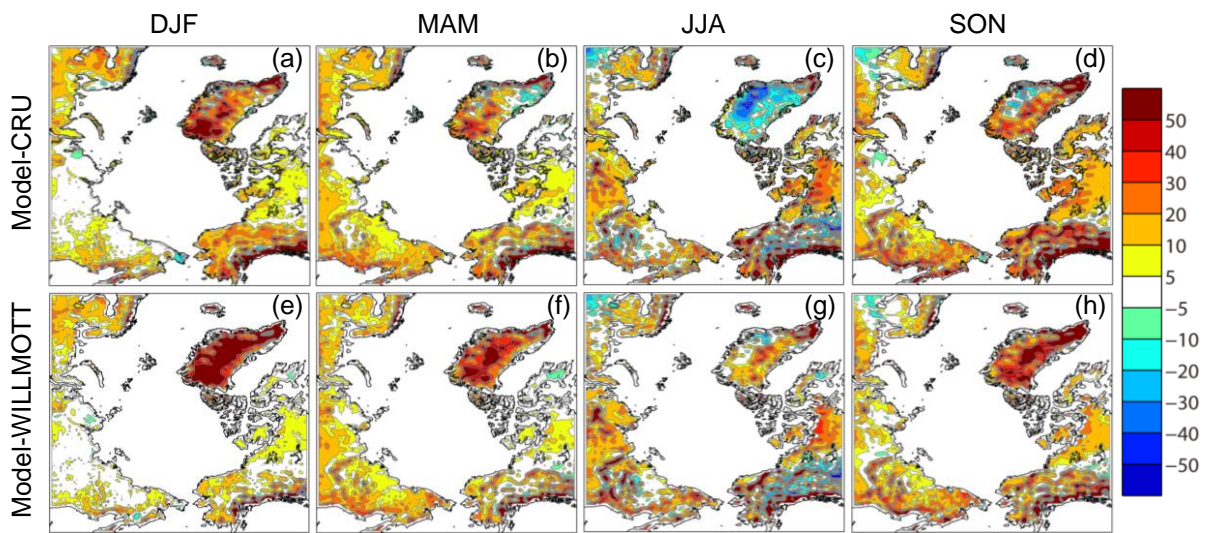
995

996

997

998

999



1000

1001 **Fig. 3.** The total seasonal precipitation anomalies (mm) relative to the CRU and WILLMOTT
 1002 datasets for the period 1961-1990. (a, e) Winter, December to February (DJF). (b, f) Spring,
 1003 March to May (MAM). (c, g) Summer, June to August (JJA). (d, h) Autumn, September to
 1004 November (SON).

1005

1006

1007

1008

1009

1010

1011

1012

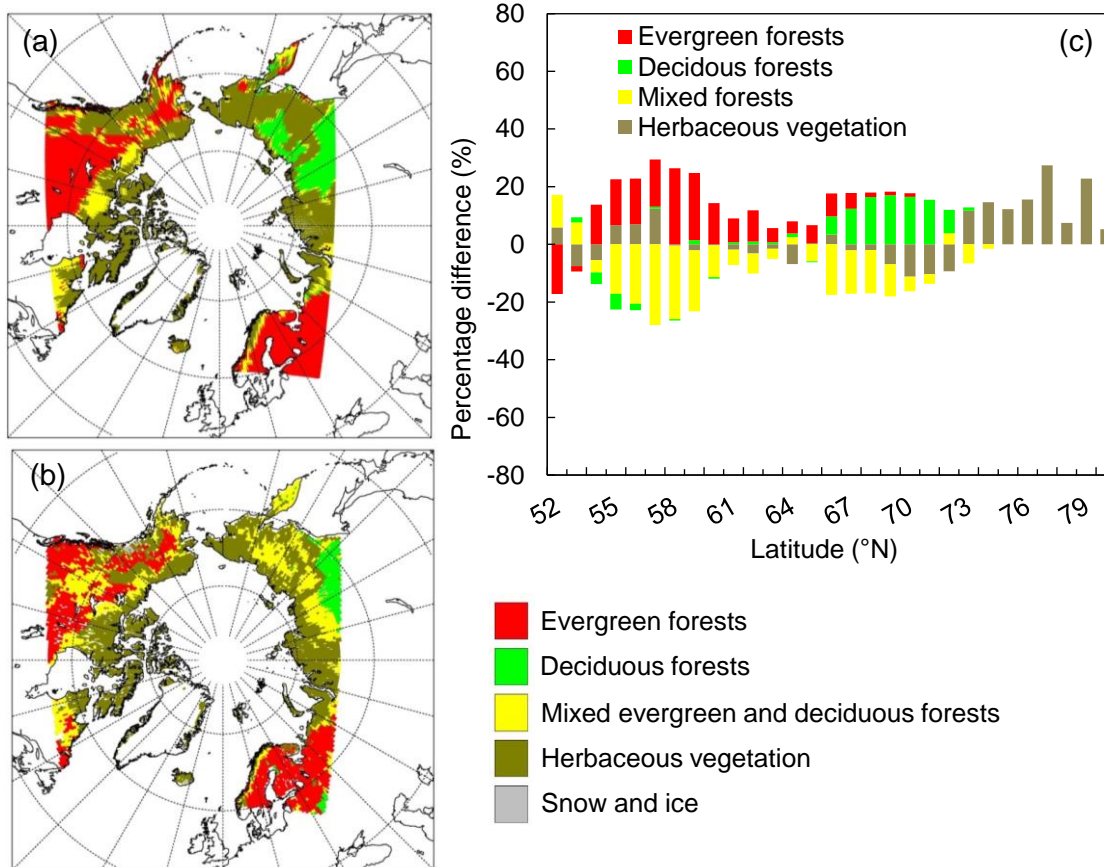
1013

1014

1015

1016

1017

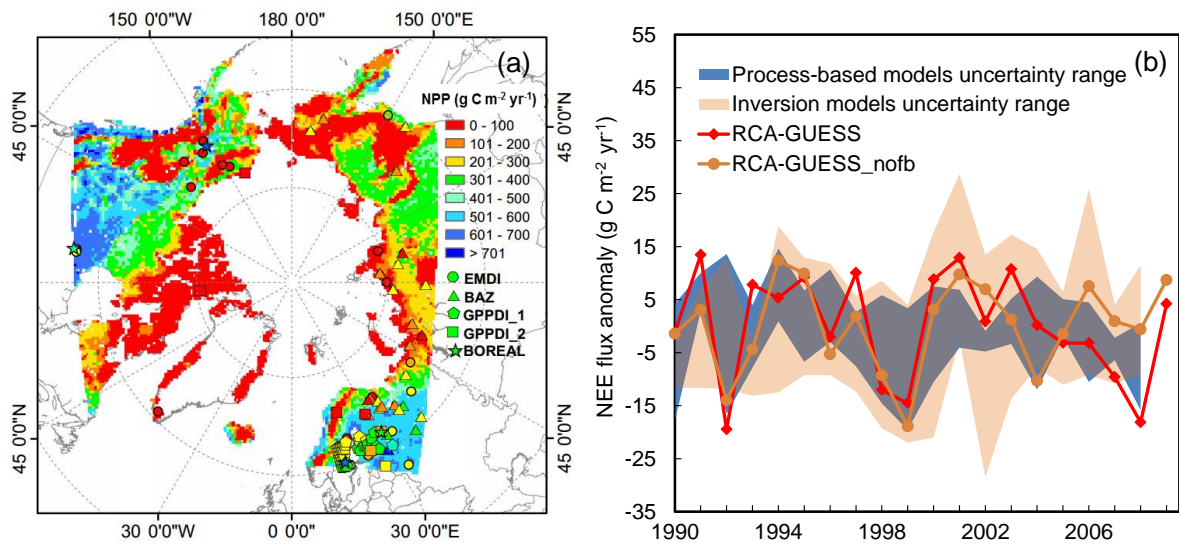


1019

1020 **Fig. 4.** The dominant potential natural vegetation (PNV) distribution comparison for the
 1021 recent period. (a) The tile-weighted PNV simulated by RCA-GUESS for the period 1961-
 1022 1990. (b) The validation map derived from the ISLSCP II Potential Natural Vegetation Cover
 1023 dataset (Ramankutty and Foley, 2010) and the Kaplan PNV map (Kaplan et al., 2003). (c)
 1024 Percentage difference (simulated minus validation map) between the number of grid cells
 1025 each aggregated vegetation class occupies in each latitude band, from 52-80 °N.

1026

1027



1028

1029 **Fig. 5.** (a) The spatial distribution of the simulated mean NPP flux for the period 1961-1990
 1030 and the NPP flux validation datasets (EMDI (Olson et al., 2013a), BAZ (Denissenko et al.,
 1031 2013), GPPDI_1 (Olson et al., 2013b), GPPDI_2 (Zheng et al., 2013), BOREAL (Gower et
 1032 al., 2012)). (b) The inter-annual variation of Arctic tundra NEE anomalies from the RCA-
 1033 GUESS feedback and non-feedback runs, the uncertainty ranges of process-based models
 1034 (LPJ-GUESS WHyMe, TEM6, TCF, Orchidee) and inversion models for the period 1990-
 1035 2009.

1036

1037

1038

1039

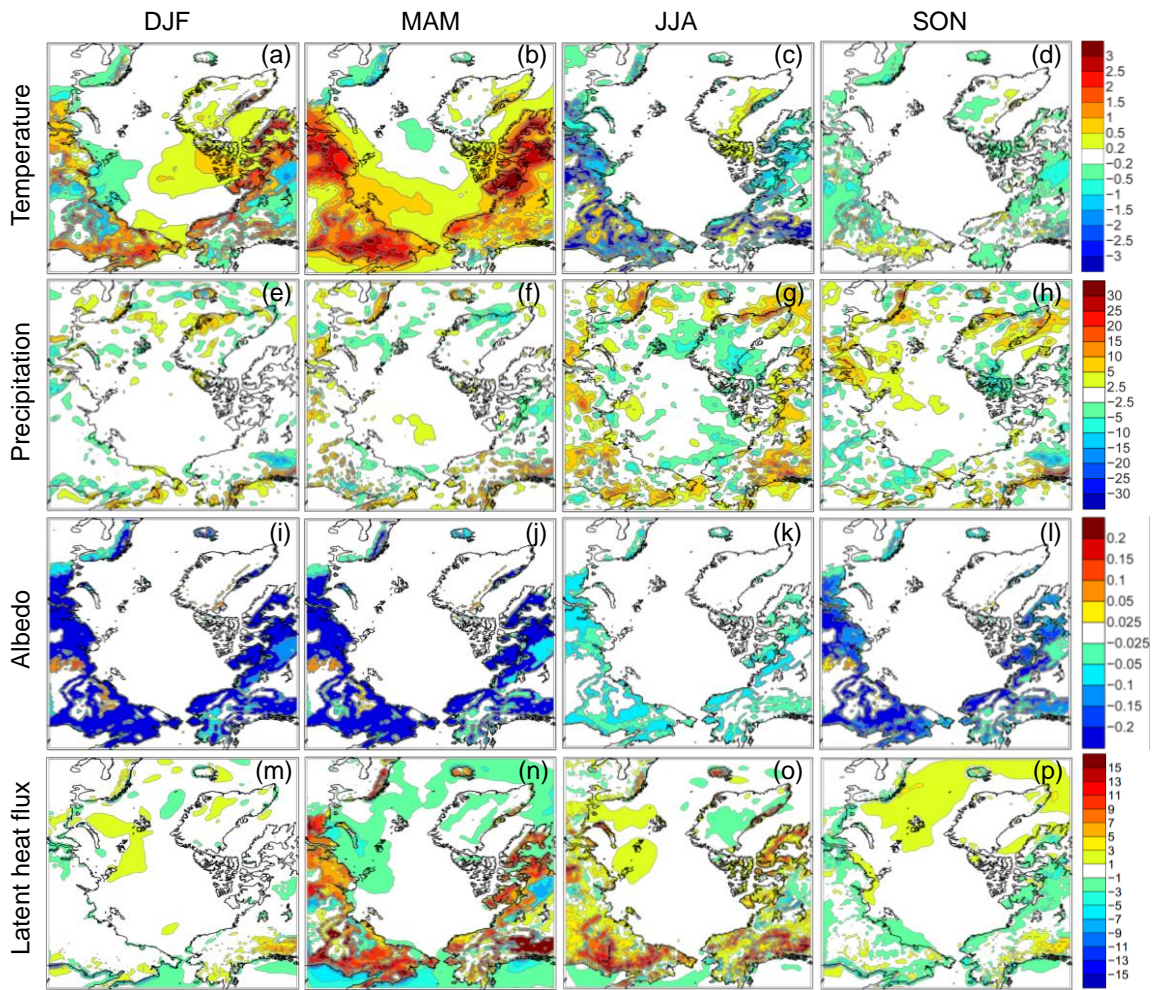
1040

1041

1042

1043

1044



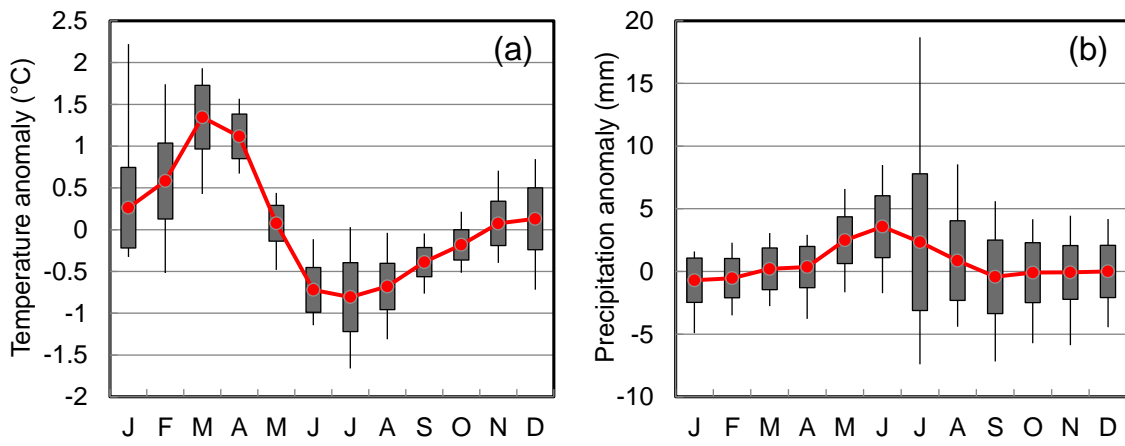
1045

1046 **Fig. 6.** The effects of biogeophysical feedbacks on 2m temperature (°C) and total
 1047 precipitation (mm), albedo (-) and latent heat flux (W m⁻²) on a seasonal basis, averaged from
 1048 2071-2100. (a, e, i, m) Winter, December to February (DJF). (b, f, j, n) Spring, Mar to May
 1049 (MAM). (c, g, k, o) Summer, June to August (JJA). (d, h, l, p) Autumn, September to
 1050 November (SON).

1051

1052

1053



1054

1055 **Fig. 7.** The seasonal cycle of (a) temperature anomalies (°C) and (b) precipitation anomalies
 1056 (mm) arising from biogeophysical feedbacks for the period 2071-2100. Each boxplot shows
 1057 the mean (red line), one SD range (black shading) and maximum and minimum values
 1058 (whiskers) for monthly climate variables.

1059

1060

1061

1062

1063

1064

1065

1066

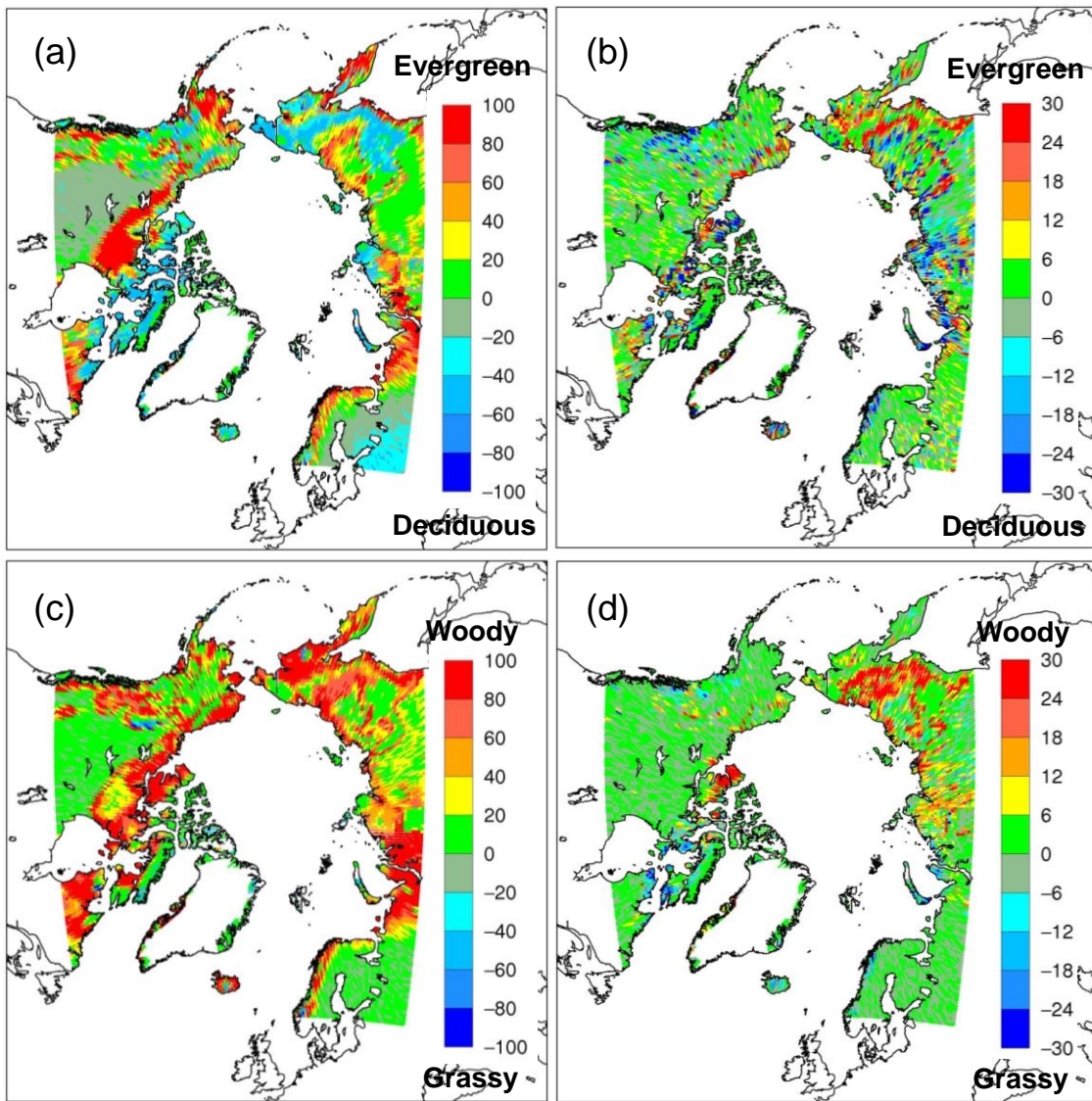
1067

1068

1069

1070

1071



1072

1073 **Fig. 8.** Normalized phenology index anomalies (%) $C_p = (LAI_{eg} - LAI_d) / (LAI_{eg} + LAI_d)$

1074 (Wramneby et al., 2010) quantified by the shift in the relative abundance between evergreen

1075 (*eg*) and deciduous (*d*) PFTs due to (a) climate change from the period 1961-1990 to the

1076 period 2071-2100; (b) the effects of biogeophysical feedbacks for the period 2071-2100.

1077 Normalized physiognomy index anomalies (%) $C_p = (LAI_w - LAI_h) / (LAI_w + LAI_h)$

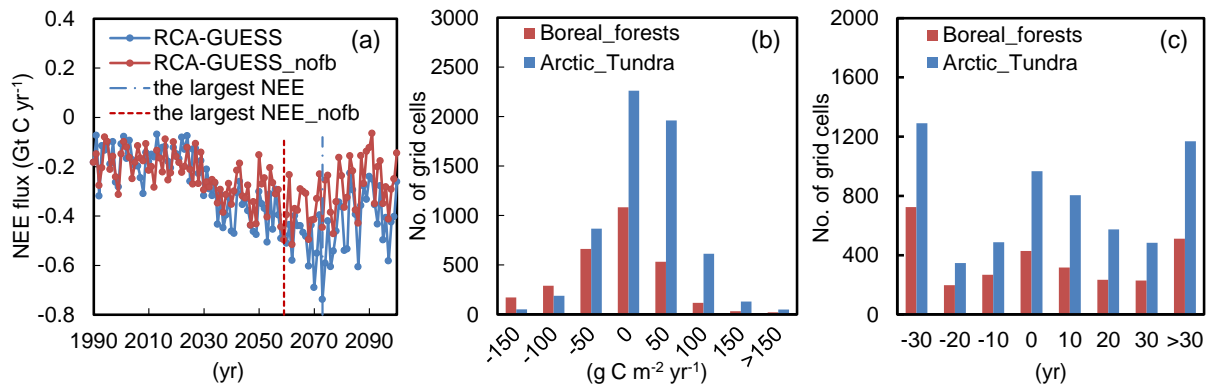
1078 quantified by the shift in the relative abundance between woody (*w*) and herbaceous (*h*) PFTs

1079 due to (c) climate change from the period 1961-1990 to the period 2071-2100; (d) the effects

1080 of biogeophysical feedbacks for the period 2071-2100.

1081

1082



1083

1084 **Fig. 9.** (a) The inter-annual variation of NEE flux (Gt C yr⁻¹) in both RCA-GUESS feedback
 1085 and non-feedback runs from 1990 to 2100 for Arctic tundra. (nofb: the non-feedback run;
 1086 negative value: carbon sink; the vertical dash and dash-dot lines denote the year with the
 1087 largest NEE over the whole period). (b) Distribution of the number of grid cells (total: 9032)
 1088 for the shift of the peak C uptake rate (g C m⁻² yr⁻¹) in both boreal forests and Arctic tundra
 1089 (positive: increase; negative: decrease) . (c) Distribution of the number of grid cells for the
 1090 shift of the year (yr) with the peak C uptake rate in both boreal forests and Arctic tundra
 1091 (positive: delay; negative: advance).

1092

1093

1094